Coupled Mo-U abundances and isotopes in a small marine euxinic basin: constraints on processes in euxinic basins

Elvira Bura-Nakic[1,2,], Morten, B. Andersen[1,3*], Corey Archer[1], Gregory F. de Souza[1], Marija Marguš[2], Derek Vance[1]

[1] Institute of Geochemistry and Petrology, Department of Earth Sciences, ETH Zürich, Clausiusstrasse 25, 8092 Zürich, Switzerland.

[2] Division for Marine and Environmental Research, Ruđer Bošković Institute, Bijenička 54, HR-10002, Zagreb, Croatia.

[3] School of Earth and Ocean Sciences, Cardiff University, Cardiff, UK.

* Corresponding author (andersenm1@cardiff.ac.uk)

~9500 words in main text

8 figures

1 table

5 supplementary tables and one supplementary text

Abstract

Sedimentary molybdenum (Mo) and uranium (U) abundances, as well as their isotope systematics, are used to reconstruct the evolution of the oxygenation state of the surface Earth from the geological record. Their utility in this endeavour must be underpinned by a thorough understanding of their behaviour in modern settings. In this study, Mo-U concentrations and their isotope compositions were measured in the water column, sinking particles, sediments and pore waters of the marine euxinic Lake Rogoznica (Adriatic Sea, Croatia) over a two year period, with the aim of shedding light on the specific processes that control Mo-U accumulation and isotope fractionations in anoxic sediment.

Lake Rogoznica is a 15 m deep stratified sea-lake that is anoxic and euxinic at depth. The deep euxinic part of the lake generally shows Mo depletions consistent with near-quantitative Mo removal and uptake into sediments, with Mo isotope compositions close to the oceanic composition. The data also, however, show evidence for periodic additions of isotopically light Mo to the lake waters, possibly released from authigenic precipitates formed in the upper oxic layer and subsequently processed through the euxinic layer. The data also show evidence for a small isotopic offset (~0.3‰ on $^{98}Mo/^{95}Mo$) between particulate and dissolved Mo, even at highest sulfide concentrations, suggesting minor Mo isotope fractionation during uptake into euxinic sediments. Uranium concentrations decrease towards the bottom of the lake, where it also becomes isotopically lighter. The U systematics in the lake show clear evidence for a dominant U removal mechanism via diffusion into, and precipitation in, euxinic sediments, though the diffusion profile is mixed away under conditions of increased density stratification between an upper oxic and lower anoxic layer. The U diffusion-driven precipitation is best described with an effective $^{238}U/^{235}U$ fractionation of +0.6‰, in line with other studied euxinic basins.

Combining the Mo and U systematics in Lake Rogoznica and other euxinic basins, it is apparent that the two different uptake mechanisms of U and Mo can lead to spatially and temporally variable Mo/U and Mo-U isotope systematics that depend on the rate of water renewal versus removal to sediment, the sulfide concentration, and the geometry of the basin. This study further emphasises the potential of combining multiple observations, from Mo-U enrichment and isotope systematics, for disentangling the various processes via which redox conditions control the chemistry of modern and ancient sediments.

1. Introduction

The sedimentary abundances and isotopic compositions of redox sensitive trace metals play a prominent role in attempts to reconstruct the history of surface Earth oxygenation. Of all the redox sensitive metals that have been used, molybdenum (Mo) and uranium (U) have perhaps been the most prominent. Both are soluble under oxidizing conditions and exhibit conservative behaviour in the open ocean, with residence times that are significantly longer than ocean mixing times (800 and 250–500 kyr respectively, Emerson and Huested, 1991). In some anoxic or euxinic (i.e. anoxic and sulfidic) settings, on the other hand, both Mo and U show non-conservative behaviour in the water column and are variably removed to sediment, though probably via different extraction mechanisms (Ku et al., 1977; Collier, 1985; McLennan, 2001; Algeo and Tribovillard, 2009; Nakagawa et al., 2012; Tribovillard et al., 2012). Organic-rich, reducing sediments are the most important modern oceanic Mo and U sinks (Emerson and Huested, 1991; Morford and Emerson, 1999; McManus et al., 2006; Scott et al., 2008). Coupled analysis of Mo and U authigenic enrichment in reducing organic-rich sediments has been used to investigate the degree of anoxia prevailing in the past water column (e.g., Scott et al., 2008; Algeo and Tribovillard, 2009; Tribovillard et al., 2012).

The Mo and parent U isotopic composition of ancient black shales are also thought to be related to the redox state of the global ocean, as Mo and U isotopes are fractionated differently in oxic and anoxic ocean sinks (e.g. Barling et al., 2001; Siebert et al., 2003; Arnold et al., 2004; Stirling et al., 2007; Weyer et al., 2008; Gordon et al., 2009; Montoya-Pino et al., 2010; Scheiderich et al., 2010; Voegelin et al., 2010; Brennecka et al., 2011a; Herrmann et al., 2012; Azrieli-Tal et al., 2014; Dahl et al., 2014; Westermann et al., 2014). The conservative behaviour of Mo in oxygenated waters arises from the fact that the main Mo species, molybdate ($Mo^{VI}O_4^{2-}$), has a low particle affinity, leading to the relatively long residence time of Mo in the oceans (Emerson and Huested, 1991). In such oxidizing environments, slow

adsorption of dissolved Mo to Mn oxide particles preferentially accumulates light Mo isotopes in the particulate phase (by ~ 3‰ for $^{98}Mo/^{95}Mo$; Barling and Anbar, 2004), leaving the dissolved Mo pool enriched in heavy Mo isotopes (Barling and Anbar, 2004). In contrast, under euxinic conditions, with significant dissolved sulfide, oxygen atoms in molybdate can be replaced with sulfur atoms (Erickson and Helz, 2000; Vorlicek and Helz, 2002). The product thiomolybdate ($Mo^{VI}O_nS_4^{2-}$) species are particle reactive, readily scavenged (e.g. by particulate Fe and organic matter), and thus removed from the water column into the underlying sediments (Helz et al., 1996; Vorlicek and Helz, 2002; Bostick et al., 2003). At sulfide concentrations greater than ~11 μmol l^{-1} the conversion of molybdate to tetrathiomolybdate ($Mo^{VI}S_4^{2-}$) is nearly complete (Erickson and Helz, 2000). Thus, in highly restricted anoxic basins, such as the Black Sea ($[\Sigma S^{-II}]$ ~300 μmol l^{-1}, Emerson and Huested 1991) the conversion of $Mo^{VI}O_4^{2-}$ to $Mo^{VI}S_4^{2-}$ is almost complete at depth, leading to near-quantitative molybdenum removal from the water column. Accordingly, in the underlying sediment, authigenic Mo records a Mo isotopic composition that is very close to the original seawater composition (Nägler et al., 2011). The process of conversion to sulfidic species does, however, involve Mo isotope fractionation (Tossell, 2005; Kerl et al., 2017), which may be expressed in mildly euxinic conditions when intermediate products in the $Mo^{VI}O_4^{2-}$ to $Mo^{VI}S_4^{2-}$ conversion are present and when conversion to tetrathiomolybdate is not complete. Furthermore, there appears to be a small isotopic difference between aqueous $Mo^{VI}S_4^{2-}$ and authigenic solid Mo, with $\Delta^{98/95}Mo_{tetrathiomo\text{-}sediment} = +0.5 \pm 0.3‰$ (Nägler et al., 2011).

Uranium, in the form of U^{6+}, mainly forms highly soluble complexes with carbonate species in oxic seawater, again leading to the relatively long residence time (Morford and Emerson, 1999). In contrast, the reduced U^{4+} species is highly insoluble. Large variations in the ratio of uranium's long-lived isotopes $^{238}U/^{235}U$ have been observed under redox-controlled U^{6+}-U^{4+} exchange in low-temperature environments (Stirling et al., 2007; Weyer et al., 2008). Oxic

adsorption of U to ferromanganese oxides without redox change, and under oxic conditions, results in a small fractionation of the $^{238}U/^{235}U$ ratio ($\delta^{238/235}U_{soln\text{-}MnOx}$ = ~0.2‰; Brennecka et al., 2011b). On the other hand, the incorporation of U^{4+} into anoxic sediments generally leads to significant (permil level) enrichment of the heavier isotope, ^{238}U, in sediment (e.g. Weyer et al., 2008; Andersen et al., 2014). In contrast to Mo, typical processes for U removal into anoxic sediments have been suggested to involve U transported with sinking particulate organic matter (Anderson et al. 1989b; Zheng et al., 2002) and diffusion of seawater U into sediment pore waters and reduction within the sediment itself (Anderson et al., 1989a; Barnes and Cochran, 1990; Klinkhammer and Palmer, 1991). Although still a matter of some debate, the latter process has been determined to dominate the authigenic U flux in most studied anoxic marine settings (e.g. Anderson 1987; McManus et al 2005). Furthermore, the mechanistic nature of U fixation within anoxic sediment is also still debated, but likely dominated by metal- and sulfate-reducing bacteria that use U^{VI} as an electron acceptor (Lovley et al., 1991; Bargar et al., 2013).

As a result, while the Mo isotopic composition of seawater may be directly recorded in sediments accumulated under strongly euxinic conditions via near-quantitative Mo uptake, U is taken up less quantitatively and U isotopes generally display large fractionations between anoxic organic-rich sediments and seawater (Weyer et al., 2008; Andersen et al., 2014; Noordmann et al., 2015; Holmden et al., 2015; Andersen et al., 2016; Rolison et al., 2017). As Mo and U display significant isotope fractionations between oxic and anoxic sinks, both isotope systems have the potential to record the redox evolution of the global ocean. However, the investigation of Mo and U behaviour in different modern settings has revealed significant Mo isotope fractionation in sediments deposited under suboxic as well as under anoxic water columns bearing low sulfide concentrations (Siebert et al., 2003; Siebert et al., 2006; Poulson et al., 2006; Poulson Brucker et al., 2009; Nägler et al., 2011). In addition to Mo removal in

127 euxinic waters, other processes have been invoked to control sedimentary Mo isotopes in
128 anoxic settings. These include the delivery of Mo with light Mo isotope compositions to
129 euxinic sediments or bottom water on Fe-Mn oxyhydroxide-rich particulates (e.g. Barling
130 and Anbar, 2004; Goldberg et al., 2009), adsorption of Mo to organic matter with an
131 isotopic fractionation (Kowalski et al., 2013) and early diagenetic redistribution of Mo
132 within sediment and pore-waters (McManus et al., 2002). Studies reporting the U isotopic
133 composition of anoxic to suboxic sediments have shown not only a significant U isotopic
134 fractionation in comparison to seawater, but also variable fractionation between these modern
135 anoxic settings. While several studies suggest an apparent U isotope fractionation factor (ε)
136 for $^{238}U/^{235}U$ in the range of ~+0.5 to 0.8‰ during U uptake in anoxic sediments (Weyer et al.
137 2008; Andersen et al., 2014; Holmden et al., 2015; Noordmann et al., 2015; Andersen et al.,
138 2016, Rolison et al., 2017) both significantly higher and lower U isotope compositions have
139 been observed in anoxic sediments (Weyer et al. 2008; Montoya-Pino et al. 2010; Noordmann
140 et al., 2015; Hinojosa et al. 2016). This suggests further mechanisms for U withdrawal from
141 the anoxic water columns, or variable U isotope mass-balance during non-quantitative
142 authigenic U sediment uptake (Andersen et al., 2017).

143 To improve our understanding of the behaviour of Mo and U and their isotopes, further
144 studies in well-characterised modern settings are needed. In this study, Mo and U
145 concentrations and isotope compositions of the water column, sinking particles, sediments and
146 pore waters of the marine euxinic Lake Rogoznica, Croatia, are presented. Based on the
147 comprehensive dataset obtained, including seasonal patterns, we shed further light on the
148 processes controlling Mo and U isotope fractionation mechanisms in anoxic water columns
149 and their sediments.

150

151 **2. Methods**

2.1. Study site

Lake Rogoznica is a small, intensely eutrophicated sea-lake situated on the eastern coast of the Adriatic Sea (Ciglenečki et al., 2005; Bura-Nakić et al., 2009; Ciglenečki et al., 2015). The lake is surrounded by sheer carbonate cliffs (4–23 m above mean sea-level), has a surface area of about 5300 m^2 and a maximum depth of ~15 m. Due to its stratification, and despite permanent water exchange with the surrounding sea through porous karst, Lake Rogoznica becomes anoxic at depth due to the remineralisation of organic matter produced in periods of intense primary production (blooms) near the surface (Ciglenečki et al., 2005; Bura-Nakić et al., 2009; Ciglenečki et al., 2015). It is therefore well-suited for studying biogeochemical processes influencing redox-sensitive trace metals. Complete vertical mixing of the lake, where cold oxygen-rich water from the surface mixes downwards and anoxic deep waters are brought to the surface, often occurs during the dry and cold autumn period. Complete mixing of the lake, leading to catastrophic anoxia in the whole water column, occurs rarely, once or twice in every 10 winters depending on the meteorological conditions (Ciglenečki et al., 2005; 2015). Under stratified conditions, the surface water is well oxygenated while the layer below approx. 9 m depth is anoxic. The anoxic deep waters become rich in sulfur (up to 5000 $\mu mol\ l^{-1}$) predominantly in the form of sulfide (Ciglenečki et al., 2005; Bura-Nakić et al., 2009; Ciglenečki et al., 2015).

2.2. Sampling and sample collection

Prior to field work, syringes, bottles, tygon tubes and all other materials used for sediment and water column sampling were pre-cleaned in ~3 N HCl and rinsed with MQ water (18 $M\Omega \cdot cm$). Unless otherwise stated, all reagents used were sub-boiling distilled twice in teflon stills.

Water column samples were collected from the middle of the lake during six campaigns spanning 2013 (February, April, July and October) and 2015 (April and July). All water samples were collected by lowering a custom-made (30 cm diameter) filter housing down into the lake, so that filtration occurred *in situ*, and the water was pumped through a 0.2 μm mesh-sized filter (Millipore, Whatman 47 mm diameter PTFE) to the surface using silicone tubing (0.9 cm outer diameter) and a Pegasus peristaltic pump. Approximately one litre was collected at each depth. All filtered samples were collected in pre-cleaned HDPE bottles and acidified (*p*H 2, using concentrated HCl). Salinity and oxygen concentration were measured *in situ* during the sampling using a HQ40D multimeter probe (HachLange, Germany). Sulfide concentrations were analysed by linear sweep voltammetry (LSV) within 8 hours of sampling according to procedures described elsewhere (Ciglenečki et al., 2005; Bura-Nakić et al., 2009; Ciglenečki et al., 2015). Electrochemical measurements were performed with μAutolab Electrochemical Instruments (EcoChemie) connected with 663VA Stand Metrohm electrode. *In situ* measurements of *p*H were performed during three sampling campaigns (October 2013, April and July 2015) using a HQ40D multimeter probe (HachLange, Germany). The *p*H values measured *in situ* were used to calculate $[H_2S]_{aq}$ following Millero et al. (1986, Supplementary Table 2).

One sediment core (~60 cm long) was collected in July 2013 from the middle and deepest part of Lake Rogoznica (~15 m) using an Uwitec gravity corer. Immediately after sampling, the core was sectioned into 5 cm segments in a glove box under N_2 overpressure. Pore water was extracted by centrifugation at 4000 rpm for 30 minutes. The pore water samples (10 to 30 ml) were transferred into HPDE bottles and acidified (*p*H 2) using concentrated HCl. A sample of the carbonate rock surrounding the lake was collected in April 2015, stored in a plastic bag, and cut into smaller pieces (1–2 g) using a diamond-blade saw.

201 **2.3. Sample preparation**

202 Chemical preparation and analysis of the samples were performed in the isotope facilities at
203 the Institute of Geochemistry and Petrology, Department of Earth Sciences, ETH Zürich,
204 Switzerland. Lake Rogoznica water column dissolved and particulates, as well as pore water
205 and sediment samples were measured for selected elemental concentrations, and Mo and U
206 isotopes. Elemental concentrations were measured in all samples (section 2.5) prior to
207 preparation for isotope composition determination.

208 Water sample aliquots (varying from 20 to 150 ml) were taken for isotopic analysis, aiming
209 for a total of 20–50 ng U and 150–250 ng Mo. These were transferred into pre-cleaned Teflon
210 jars for the isotope determination, and spiked with the IRMM–3636 ^{236}U–^{233}U double-spike
211 (Richter et al., 2008) aiming for a $^{236}U/^{235}U$ of ~4, and a ^{100}Mo–^{97}Mo double-spike (Archer
212 and Vance, 2008) aiming for a 1:1 spike to sample ratio. These water sample aliquots were
213 subsequently dried down (all at 100 °C). Due to the high Na–content, a large NaCl precipitate
214 would form during this step. To obtain a more pure metal fraction, samples were leached
215 using 10 ml 7 N HCl for 24 hours, a treatment which dissolves Mo, U and other metals but
216 minimises dissolution of NaCl. The samples were then centrifuged (3500 rpm for 10 minutes),
217 and the supernatant taken for analysis. The recoveries of both U and Mo in the supernatant
218 were consistently >90% using this procedure. The supernatant was then dried down and re-
219 dissolved in 5 ml 7 N HCl in preparation for column chromatography.

220 Filters used for the water filtration were dissolved in 10 ml of concentrated HNO_3 in pre-
221 cleaned 60 ml Teflon beakers and dried down (all at 100 °C). Samples were then re-dissolved
222 and fluxed in a 2 ml mixture of conc. HNO_3 and H_2O_2 (Merck Superpure, 1:1 ratio) on a
223 hotplate for 24 hours, before being dried down. They were then re-dissolved in 5 ml of 7 N
224 HCl and an aliquot (100 µL) was taken to determine elemental concentrations. The filters held
225 28 to 148 ng Mo and 3 to 23 ng U, while the total blanks for dissolution of clean unused

filters in the same manner were ~40 pg for Mo and <1 pg for U (Supplementary Table 1). The samples were spiked with the U and Mo double-spikes as described above, and left in closed Teflon beakers to equilibrate on a hotplate (100 °C) before column chromatography.

The pore water samples were weighed, dried down in pre-cleaned Teflon beakers, and pre-treated with the mixture of concentrated HNO_3 and H_2O_2 in a 1:1 ratio on a hotplate for 24 hours. Samples were then re-dissolved in 5 ml 7 N HCl and an aliquot taken to determine the elemental concentrations. Samples containing 70–170 ng Mo and 4–35 ng U were then spiked with the U and Mo double-spikes and left to equilibrate on a hotplate in preparation for column chromatography.

Approximately 50–100 mg of the sediment samples was used for analysis. Full dissolution of sediments was carried out using conventional protocols for silicates, involving mixtures of HF–HNO_3–HCl and H_2O_2 in the same manner described in Andersen et al. (2013). After final dissolution in 10 ml 6 N HCl, an aliquot was taken to determine elemental concentrations. An aliquot containing 20–50 ng U and 150–250 ng Mo was added to pre-cleaned Teflon beakers, spiked with the U and Mo double-spikes, and then left to equilibrate on a hotplate before being dried down (all at 100 °C). Samples were then re-dissolved in 5 ml 7 N HCl in preparation for column chromatography.

The carbonate rock sample was weighed and dissolved in a pre-cleaned Teflon beaker. The initial carbonate rock dissolution was performed in a 5 ml mixture of conc. HCl and H_2O in a 1:1 ratio for 24 hours. The sample was then dried down and pre-treated on a hotplate for 24 hours with a mixture of conc. HNO_3 and H_2O_2 in a 1:1 ratio. After final dissolution in 10 ml of 0.3 N HNO_3 an aliquot was taken to determine elemental concentrations. An aliquot containing ~50 ng U was added to a pre-cleaned Teflon beaker, spiked with the U double-spike, left to equilibrate on a hotplate before being dried down at 100 °C. The sample was then re-dissolved in 5 ml 7 N HCl in preparation for column chromatography.

2.4. Column chromatography

A one step purification and U–Mo separation procedure was conducted using RE Resin (Triskem technologies) in custom-made shrink-fit Teflon columns (~0.2 ml resin reservoir). Prior to sample loading, resin was added to the columns, pre-cleaned using 2 ml of a mixture 0.1 N HCl–0.3 N HF, rinsed with MQ water, and pre-conditioned with 2 ml 7 N HCl. Samples were then loaded in 5 ml 7 N HCl and the matrix eluted with 10 ml 1 N HCl. The Mo and U fraction were eluted separately, first with 5 ml 0.2 N HCl and then 5 ml of a 0.1 N HCl–0.3 N HF mixture, respectively. The column chromatography protocol yielded highly pure Mo and U fractions with only traces of major or minor elements. For example, abundant cations in the pre-column extracted seawater – e.g. Mg (~1000 ppm) and Ca (~400 ppm) – were present at less than 100 ppb in the purified Mo and U fractions. Column blanks were <13 pg and <22 pg for Mo and U, respectively (Supplementary Table 1). The U fractions were fluxed on a hotplate for 24 hours in a 1 ml mixture of concentrated HNO_3 and H_2O_2 in 1:1 ratio, to oxidise any resin bleeding into the sample cut during chemistry, and dried down. The purified Mo and U were then re-dissolved in 0.3 N HNO_3 and 0.2 N HCl, respectively, for mass spectrometry.

The column separation procedure was tested by processing two open Atlantic Ocean samples for U and Mo, following the dissolution and column chemistry procedure described above. The isotopic compositions of Mo and U measured are in good agreement with previously reported values (see below and Supplementary Table 1) (Siebert et al., 2003; Weyer et al., 2008; Nakagawa et al., 2012; Andersen et al., 2014; Tissot and Dauphas, 2015).

2.5. Elemental concentration measurements

The concentrations of selected elements (see Supplementary Table 2) were measured in 0.3N HNO_3 using a Thermo–Finnigan Element XR ICP–MS, following the same measurement protocol as outlined in Andersen et al. (2013, 2016). In brief, the instrument set-up included both low and medium resolution, using a primary in-house concentration standard interspersed with measurements of three unknowns and a secondary standard (BCR–2). The BCR–2 standard was used to monitor the accuracy and reproducibility. Repeated measurements of BCR–2 gave a reproducibility better than ± 10% (1 S.D.) and mean values within ± 10% of the certified concentrations (see Andersen et al., 2016).

2.6. Molybdenum and uranium isotope measurements

Isotope ratios were measured on a Neptune (Thermo–Finnigan) MC–ICPMS equipped with an AridusII auto-sampler (CETAC) using a PFA nebulizer and spray chamber (CPI) sample introduction system. Details of instrumental set-up are given in Archer and Vance (2008) for Mo isotopes and Andersen et al. (2016) for U isotopes. Molybdenum isotope ratios are presented as $\delta^{98}Mo = [^{98/95}Mo_{sample}/^{98/95}Mo_{standard} - 1] \times 1000$. All Mo isotope compositions for samples are reported relative to NIST SRM 3134 = +0.25‰ (Nägler et al., 2014). Uranium isotope ratios are reported relative to the CRM–145 standard and presented as $\delta^{238}U = [^{238/235}U_{sample}/^{238/235}U_{standard} - 1] \times 1000$ and as ($^{234}U/^{238}U$) activity ratios compared to secular equilibrium (Cheng et al., 2013).

The Mo double spike method was verified via the analysis of an in-house CPI standard as well as open-ocean seawater. During the period of this study, analysis of our in-house CPI standard with standard/spike ratios in the range of 0.1 to 5 gave $\delta^{98}Mo$ = -0.02± 0.04‰ (all isotope data reported as 2 S.D., Supplementary Table 1) relative to NIST SRM 3134 = +0.25‰. Four seawater samples gave $\delta^{98}Mo$ of +2.37 ± 0.03‰, in perfect agreement with previous data for

298 seawater δ^{98}Mo (Siebert et al., 2003; Nakagawa et al., 2012). The verification of the U double
299 spike method was carried out via repeated measurements of the in-house CZ–1 uraninite
300 standard and five open-ocean seawater samples (Supplementary Table 1). The long-term
301 average and ±2 S.D. reproducibility for the CZ–1 standard were –0.04 ± 0.07‰ for δ^{238}U and
302 0.9996 ± 0.0025 for (^{234}U/^{238}U) (Supplementary Table 1), in agreement with previously
303 reported values (Stirling et al., 2007; Andersen et al., 2015; 2016). Uranium isotopic analysis
304 of five seawater samples gave a δ^{238}U = –0.39 ± 0.04‰ and (^{234}U/^{238}U) = 1.147 ± 0.003,
305 again in very good agreement with reported data for seawater (Weyer et al., 2008; Andersen et
306 al., 2010; 2014; Tissot and Dauphas, 2015). Finally, a set-up measuring samples with low U
307 (2–10 ng) amounts equivalent to some filter samples, yielded δ^{238}U = –0.02 ± 0.23‰ and
308 (^{234}U/^{238}U) = 0.999 ± 0.018 for the CZ–1 standard (Supplementary Table 1).

309

310 **3. Results**

311 **3.1. General chemical characterisation of the water column**

312 Salinity, oxygen ([O_2]), sulfide ([ΣS^{-II}]), particulate Fe ([Fe]$_{part}$) and particulate Mn ([Mn]$_{part}$)
313 in the water column are presented in Supplementary Table 2 and summarised in Figure 1.
314 During the study period (2013 and 2015) the lowest salinity recorded was during winter and
315 spring due to increased precipitation and decreased evaporation during the colder season of
316 the year. The position of the halocline is temporally variable, from approx 5 to 9 m. Oxygen
317 concentrations are strongly inversely correlated with the [ΣS^{-II}], the latter reaching the highest
318 concentration of ~5 mmol l^{-1} in summer 2013 at 13 m depth. Particulate Fe and Mn are higher
319 at the chemocline and in the deeper anoxic waters than in the upper oxic layer.

320

321 **3.2. Molybdenum in the water column and settling particles**

Depth profiles of salinity-normalised (to 35) dissolved Mo ($[Mo]_{SNdiss}$) and of particulate Mo ($[Mo]_{part}$), as well as their $\delta^{98}Mo$, are presented in Supplementary Table 2 and Figure 2. The $[Mo]_{SNdiss}$ is higher than the measured [Mo] by 3 to 50% in the upper oxic waters ($O_2 > 5$ mg l^{-1}) that are influenced by precipitation, but the correction has little impact on the deeper anoxic waters. The $[Mo]_{SNdiss}$ profiles show a strong depth gradient, mirroring changes in the redox conditions in the water column. With the exception of very high [Mo] in surface waters in April and July 2013, [Mo] generally varies between ~100 nmol l^{-1} in the oxic and ~10 nmol l^{-1} in the deeper euxinic waters. The shape of the profiles is rather different for the first three sampling dates (February-July 2013) versus the last three (Oct 2013, April 2015, July 2015). The latter three profiles show a much sharper transition across the chemocline and much more homogeneous concentrations within each redox regime – the upper oxic layer and the lower euxinic layer. For the later three sampling times, $[Mo]_{part}/[Mo]_{diss}$ is homogeneously low in the upper oxic water column (generally ≤ 0.01) and higher in the lower anoxic portion (up to 0.19). The first three sampling events are also much more heterogeneous in this ratio.

Lake Rogoznica waters generally show dissolved Mo isotopic composition ($\delta^{98}Mo_{diss}$) in the range +2.2 to +2.5 ‰ (Fig. 2). The exception is April 2013 and the top of the water column in July 2013, where values are much more variable and extend down to +0.8‰. The isotopic composition of the particulate Mo ($\delta^{98}Mo_{part}$) spans a wide range, from $\delta^{98}Mo$ = +0.1 to +2.1‰. In the anoxic water column the particles were generally more enriched in heavy Mo isotopes ($\delta^{98}Mo_{part}$ from +0.6 to +2.0‰) in comparison with those from the oxic water column (from +0.1 to +1.8‰).

3.3. Uranium in the water column and settling particles

Salinity normalised ($[U]_{SNdiss}$) and particulate ($[U]_{part}$) U concentrations, as well as $\delta^{238}U$, are presented in Supplementary Table 3 and Figure 2. As with Mo, the salinity normalisation increases the $[U]_{SNdiss}$ by 2 to 50% in the upper oxic waters influenced by precipitation, but has little influence on the deeper high salinity anoxic waters. The deeper anoxic waters are depleted in dissolved U ($[U]_{diss}$: 1.4 to 3.4 nmol l^{-1}) compared to the oxic surface layer (8.9 to 11.2 nmol l^{-1}). Dissolved [U] decreases towards the bottom for all 6 sampling campaigns. Particulate U concentrations (normalised to the water volume the filters were extracted from) are generally low, ranging from 0.01 to 0.1 nmol l^{-1} during the whole sampling period, and show no significant seasonal variation. Particulate U concentrations are consistently higher within the anoxic waters column, reaching a maximum at the chemocline and the bottom of the lake. The $[U]_{part}/[U]_{diss}$ is significantly lower than the $[Mo]_{part}/[Mo]_{diss}$ ratio, reaching max values of 0.004 for the oxic water column and 0.03 for anoxic water column samples.

Data for the uranium isotopic composition of the dissolved pool ($\delta^{238}U_{diss}$) show lighter values than that for open-ocean seawater ($\delta^{238}U$ = -0.39‰, Supplementary Table 1), ranging from –0.5 to –1.1‰ and with generally lower values with depth. The isotopic composition of particulate U ($\delta^{238}U_{part}$) is in the range –0.2‰ to –1.5‰, with the lowest $\delta^{238}U_{part}$ recorded in July 2013 at 6m depth, near the chemocline. $(^{234}U/^{238}U)_{diss}$ was in the range 1.111 to 1.148 and $(^{234}U/^{238}U)_{part}$ in the range 1.101 to 1.152 (Supplementary Table 3).

3.4. Molybdenum and uranium in the sediments and pore water

Mo and U concentrations ($[Mo]_{bulk}$, $[U]_{bulk}$) and isotopic compositions ($\delta^{98}Mo_{bulk}$, $\delta^{238}U_{bulk}$) in the anoxic sediments are presented in Supplementary Table 4 and Fig. 3.

These bulk data were used to calculate authigenic abundances using the measured Al, Mo and U in the sediment samples (Supplementary Table 4) and assumed lithogenic Mo/Al and U/Al ratios of 1.1×10^{-5} g g^{-1} and 1.8×10^{-5} g g^{-1}, respectively (Taylor and McLennan, 1985; Tribovillard et al., 2006; Andersen et al., 2014). For the isotopic composition of the detrital component a $\delta^{98}Mo_{det}$ of +0.3‰ (Voegelin et al., 2014) and a $\delta^{238}U_{det}$ of -0.3‰ (Andersen et al., 2016), were used, with:

$$\delta^{98}Mo_{auth} = \frac{(\delta^{98}Mo_{bulk}[Mo]_{bulk} - \delta^{98}Mo_{det}[Mo]_{det})}{[Mo]_{auth}} \quad [1]$$

$$\delta^{238}U_{auth} = \frac{(\delta^{238}U_{bulk}[U]_{bulk} - \delta^{238}U_{det}[U]_{det})}{[U]_{auth}} \quad [2]$$

Using this approach, the detrital Mo contribution to the sedimentary budget is found to be minimal, so that more than 99% of the Mo in the sediments has an authigenic origin. Thus, the impact of the detrital fraction on the measured bulk Mo isotopic composition of the sediment is also negligible. For the bulk U there is a higher contribution of detrital U (from 10 to 23%). Accordingly, the calculated authigenic $\delta^{238}U$ is shifted towards slightly lower values (by up to 0.03‰) relative to the bulk sediment. The measured ($^{234}U/^{238}U$) ratio in the samples, along with an assumption that the detrital material is in secular equilibrium (~1) and that the authigenic U has a ratio = 1.147 like modern seawater, provides an alternative method for performing the detrital U correction. The sediments display high ($^{234}U/^{238}U$), ranging from 1.096 to 1.120, demonstrating the predominance of authigenic U. Removal of the detrital U

390 component from the bulk using ($^{234}U/^{238}U$), leads to corrected $\delta^{238}U$ authigenic values that are
391 essentially the same as those obtained using the U/Al method (see Supplementary Table 4).

392 The $[Mo]_{auth}$ and $[U]_{auth}$ were in the range 11 to 80 μg g^{-1} and 2.4 to 7.3 μg g^{-1},
393 respectively, implying moderate Mo and U enrichments in the anoxic sediments. The
394 $\delta^{98}Mo_{auth}$ is variable (1.6 to 2.2‰), but is consistently lower than the average oceanic
395 $\delta^{98}Mo$ composition (+2.36 ± 0.10‰, Siebert et al., 2003). Sedimentary $\delta^{238}U_{auth}$ is, on
396 average, slightly higher (~0.15‰) than the average oceanic $\delta^{238}U$ (–0.39‰), with the
397 exception of the sample from 17.5 cm ($\delta^{238}U_{auth}$ = –0.42 ± 0.07‰). The sedimentary
398 ($^{234}U/^{238}U$) shows no significant variability throughout the investigated core
399 (Supplementary Table 4). The measured host carbonate rock sample gave a $\delta^{238}U$ = –0.16
400 ± 0.04‰, a ($^{234}U/^{238}U$) of 1.012, a $[U]_{bulk}$ of 1.12 μg g^{-1} and $[Mo]_{bulk}$ of 0.72 μg g^{-1}
401 (Supplementary Table 4).

402 Pore water Mo and U concentrations ($[Mo]_{pw}$, $[U]_{pw}$) (Supplementary Table 5, Fig. 3)
403 were consistently low throughout the core, with average $[Mo]_{pw}$= 5 ± 1 nmol l^{-1} and $[U]_{pw}$
404 = 0.17 ± 0.04 nmol l^{-1} (n=13). The $\delta^{238}U_{pw}$ closely resembles the $\delta^{238}U_{diss}$ recorded in the
405 deepest anoxic bottom waters ($\delta^{238}U_{diss}$ in the range –0.9 to –1.1‰). In contrast, pore
406 water Mo is slightly enriched in the heavier Mo isotopes, with an average $\delta^{98}Mo_{pw}$ of
407 +2.48 ± 0.08‰ (n=13), in comparison to $\delta^{98}Mo_{diss}$ in anoxic bottom waters (see Figures 2
408 and 3).

409

410 **4. Discussion**

411 **4.1 Behaviour of Mo and its isotopes in Lake Rogoznica**

412 ***4.1.1 Water column Mo behaviour***

413 The depth profiles for Mo and its isotopes in Fig. 2 split into two types of behaviour. The
414 dissolved Mo concentration profiles for October 2013 to July 2015 closely resemble those
415 previously reported from Lake Rogoznica (Helz et al., 2011), in showing a sharp transition
416 across the chemocline from high in the oxic portion above to low in the anoxic part of the lake
417 below. Profiles between Feb 2013 and July 2013, on the other hand, show more unexpected
418 behaviour. Below we discuss these anomalous features first, before moving on to the more
419 "typical" features of the later three sampling campaigns.

420 The first three sampling campaigns, and in particular April and July 2013, are often
421 characterised by very high Mo concentrations ($[Mo]_{SN}$ up to 577 nmol l^{-1}) in oxic surface
422 waters. (Fig. 2). Moreover, although these profiles exhibit the expected decrease of dissolved
423 Mo in anoxic waters, concentrations at depth are up to 2.5 times higher than in the later three
424 sampling campaigns. These high dissolved Mo concentrations are associated with generally
425 lower $\delta^{98}Mo_{diss}$, both in the oxic upper water column (as low as +0.75 ± 0.02‰) and in the
426 deep euxinic portion (as low as +1.32 ± 0.02‰). Combined, these observations suggest an
427 additional source of isotopically light Mo to the water column before or during this period.
428 For the oxic part of the water column, the Mo abundance and isotopic data are mostly
429 explained by the mixing of a "normal" signature, typified by the analyses from October 2013
430 to July 2015, with an additional Mo source that has a $\delta^{98}Mo$ of around +0.4 to +0.5‰ (Fig.
431 4a).

432 The origin of this additional Mo source is more difficult to identify. The Mediterranean
433 generally sees unusually high dust supply from the Sahara (Prospero, 1996), and one
434 possibility is that the additional Mo derives from such a source. The Mo associated with dust
435 is most likely to be associated with Fe-Mn oxyhydroxide-rich surfaces, which have the
436 required light isotope compositions (e.g. Barling and Anbar, 2004; Goldberg et al., 2009).
437 It is notable that the reservoir of Mo in particulates is also high, by one or two orders of

magnitude, during the anomalous sampling periods. The $\delta^{98}Mo_{part}$ is also consistently lower than during the last three sampling campaigns, particularly in the upper oxic water column where the difference between the dissolved and particulate loads ($\Delta^{98}Mo_{diss\text{-}part}$) is up to +2.2‰ in the first three samplings versus a maximum of +1.3‰ in the second three. The suggested dust source is not strongly supported by particulate Al, Fe and Mn concentrations which, though variable through time and space, are not particularly strongly correlated with high Mo concentrations or light Mo isotopes. On the other hand, if dust particles fall quickly through the water column while their impact lingers in the dissolved pool, or if Mo on Fe-Mn coatings is particularly soluble relative to Fe and Mn, such a correlation might not necessarily be expected.

Another potential Mo source could, in principle, be leaching of Mo from the surrounding carbonate karst. However, Mo concentration in the carbonate rock sample measured was low (0.71 μg g^{-1}, Supplementary Table 4), in agreement with previously reported values for carbonate (Vogelin et al., 2009, 2010). The main reservoir of Mo in the carbonate host rock is also likely to be Fe-Mn oxyhydroxide coatings. The vertical position of the halocline in Lake Rogoznica shifts seasonally, and during winter 2013 it was situated at a relatively shallow level (3 to 4 m depth). This may have allowed anoxic waters to enter into karst channels and dissolve Fe-Mn oxyhydroxide coatings on carbonate. Finally, the vertical position of the chemocline in Lake Rogoznica also varies, by 2-4m, again depending on season and meteorological conditions. Such temporal variation may also periodically expose Mo sequestered to Fe-Mn oxyhydroxides, in recently deposited unconsolidated sediment in the oxic portion of the lake, to reductive dissolution.

During the last three sampling campaigns dissolved salinity-normalised Mo concentrations in the upper 5m of the water column are, at 97±5 nmol kg^{-1}, close to the mean oceanic $[Mo]_{diss}$ value (107 ± 7 nmol l^{-1}, Collier, 1985; Nakagawa et al., 2012). In

addition, the average $\delta^{98}Mo_{diss}$ for these samples is +2.16 to 2.34‰, similar to the measured average oceanic dissolved pool $\delta^{98}Mo$ signature ($\delta^{98}Mo$= +2.37 ± 0.03‰, Supplementary Table 1). The $\delta^{98}Mo_{part}$ ranged from +0.98 to +1.68‰ in the oxic surface waters and $\delta^{98}Mo_{diss\text{-}part}$ = 0.65-1.53‰. This difference is consistent with a dominant role for amorphous Fe (oxyhydr)oxides (e.g. ferrihydrite, goethite), which have been shown experimentally to exhibit fractionations relative to dissolved Mo in the range of 1.1 to 1.4‰ (Goldberg et al., 2009).

At the chemocline, $[Mo]_{diss}$ decreases and reaches steady concentrations of about 9 nmol l^{-1} in the anoxic (O_2~0 mg l^{-1}) waters below, a behaviour previously observed both at Lake Rogoznica (Helz et al., 2011), and in other modern euxinic basins (Emerson and Huested, 1991; Colodner et al., 1995; Algeo and Tribovillard, 2009; Nägler et al., 2011). In all the profiles there are minor but significant excursions in $\delta^{98}Mo$ of the dissolved pool close to the chemocline. For example, in October 2013 and April 2015, $\delta^{98}Mo_{diss}$ shows a slight increase, by about 0.3‰, just at and below the chemocline and at depths where significant removal of dissolved Mo starts. Just beneath this, $\delta^{98}Mo_{diss}$ decreases again and the deepest samples are again close to those in oxic waters, at $\delta^{98}Mo_{diss}$ = +2.31±0.14‰. The July 2015 campaign does not record the initial increase as Mo concentrations begin to drop with depth. Particulate Mo concentrations increase beneath the chemocline, and though they stay beneath 2 nmol l^{-1}, the $[Mo]_{part}/[Mo]_{diss}$ ratio increases to values as high as 0.2. The $\Delta^{98}Mo_{diss\text{-}part}$ decreases with depth, with $\delta^{98}Mo_{part}$ compositions up to +2.03‰ in the deeper anoxic water column.

To our knowledge, the only other study reporting $\delta^{98}Mo$ values for sinking particles formed in anoxic water columns is that for Lake Cadagno, Switzerland, in Dahl et al. (2010). This study hypothesised that $\Delta^{98}Mo_{diss\text{-}part}$ in anoxic waters is a function of both

$[H_2S]_{aq}$ and the time available for equilibration between particles and water versus the scavenging lifetimes of intermediate thiomolybdate species. In this view, when sulfide levels are low enough for non-quantitative transformation of molybdate to tetrathiomolybdate, and for rapid scavenging timescales for intermediate thiomolybdate species, isotopic differences are expected between residual dissolved Mo and particulate Mo (Tossell, 2005; Kerl et al., 2017).

Consistent with this view, the data for $\Delta^{98}Mo_{diss\text{-}part}$ within the water column of Lake Rogoznica does exhibit a strong relationship with total dissolved sulfide (Fig. 4b). But the relationship appears to become asymptotic to a value of about +0.3‰ at very high dissolved sulfide levels. It is possible that general conclusions regarding the behaviour of Mo and its isotopes in euxinic water columns from these Lake Rogoznica data are complicated by the potential impact of Fe-Mn oxyhydroxide particulates, discussed earlier with reference to the first three sampling campaigns. For example, it is possible that the small excursions near the chemocline could be caused by oxidative-reductive cycle involving Fe-Mn oxyhydroxides. Such a rationale is not, however, consistent with all the details of the data. Thus, the small increase in $\delta^{98}Mo_{diss}$ just below the chemocline, where Mo is first removed from the water column, is the opposite to that which might be expected if isotopically light Fe-Mn oxyhydroxides were sinking into the euxinic layer and undergoing reductive dissolution. Rather this feature, coupled to increases in the Mo_{part}/Mo_{diss} ratio, is much more readily explained in terms of preferential and non-quantitative removal of light Mo isotopes to particulates due to formation of intermediate thiomolybdates at low dissolved sulfide concentrations. Thus, although the exact value of $\Delta^{98}Mo_{diss\text{-}part}$ in the anoxic water column is difficult to estimate from our data set, it is very likely that the removal of Mo from the anoxic water of Lake Rogoznica is associated

511 with minor Mo isotope fractionation, similar to that already observed in Kyllaren Fjord,
512 Black and Baltic Sea anoxic water columns (Nägler et al., 2011; Noordmann et al., 2015).
513
514 ***4.1.2 Mo and its isotopes in sediment and pore water***
515 As noted in Section 3, the detrital Mo component of anoxic Lake Rogoznica sediments is very
516 small, and more than 99% has an authigenic origin. The overall $\delta^{98}Mo_{auth}$ is high (Fig. 3),
517 ranging from +1.6 to +2.2‰, and with an average of 1.95 ± 0.17‰, (n=13, 1SD). The
518 dissolved-particulate difference for sediment-pore water pairs shows a more scattered
519 relationship with total dissolved sulfide than data for the water column (Fig. 4b). It is
520 again the case, however, that $\Delta^{98}Mo_{diss\text{-}part}$ is never zero, and the minimum values
521 observed are again about 0.3‰, similar to the water column. This overall finding is again
522 consistent with the previous suggestion in Nägler et al. (2011) that $\Delta^{98}Mo_{diss\text{-}part}$, even for
523 near-quantitative removal to sediment at high sulfide concentrations, does involve a small
524 fractionation.
525 On the other hand, sediments at Lake Rogoznica are again more complicated than such a
526 simple picture can explain. Dissolved sulfide levels in the pore waters of Lake Rogoznica
527 are very high, and equilibration times in the sediment are presumably long. Thus, the
528 occasionally high values of $\Delta^{98}Mo_{diss\text{-}part}$ are difficult to explain without invoking some
529 temporal variation in redox conditions. Most of the time, Lake Rogoznica waters are
530 characterised by a sharp chemical gradient and an anoxic layer with high $[H_2S]_{aq}$ at
531 depths >8–9 m, but seasonal mixing is known to occur during particularly dry and cold
532 autumn periods (Ciglenečki et al., 2005; Helz et al., 2011; Ciglenečki et al., 2015).
533 During these periods cold oxygenated waters slowly sink towards the bottom, causing
534 contraction of the anoxic layer so that anoxic conditions are restricted to the deep

nepheloid layer (~13 m, Helz et al., 2011). The last two such complete mixing events occurred in 2011 and 1997 (Ciglenečki et al., 2005; Ciglenečki et al., 2015). After these events, anoxia is re-established, potentially causing reductive dissolution of Fe-Mn (oxyhydr)oxides deposited at the bottom of the lake during mixing events (Helz et al., 2011). We speculate that, after these events, Lake Rogoznica bottom waters are most probably enriched in light Mo isotopes, which could potentially affect the isotopic composition of Mo extracted from such waters.

4.2 Behaviour of U and its isotopes in Lake Rogoznica

4.2.1 Uranium and its isotopes in the water column

Previous studies from the two major modern semi-restricted euxinic basins (Cariaco Basin and Black Sea) have suggested that in such settings U is not removed to sediment through processes in the water column, but rather via reduction in sediment driving U diffusion from the overlying waters into the sediments (Anderson, 1987; Anderson et al., 1989a). The first-order features of the Lake Rogoznica data can first be assessed in terms of this paradigm, in the interests of ascertaining whether it is generally applicable to euxinic basins of different sizes and, for example, at the very high dissolved sulfide concentrations seen in Lake Rogoznica.

Focusing first on U concentration, the above scenario implies no removal term in the water column, so that water column depth profiles should be explained in terms of diffusion and advection processes alone. In a simplified diffusion-advection-reaction framework the precise shapes of [U] depth profiles will be dependent on the rate of U diffusion into sediment compared to the rate at which the water column is mixed by advection. Here we assess

whether such a simplified model explains the first order features of the [U] data for Lake Rogoznica.

At steady-state, any depth profile in the lake can be modelled using the ADR equation:

$$D_z \frac{d^2C}{dz^2} - \omega_z \frac{dC}{dz} - kC = 0 \qquad [3]$$

where z is depth, D is the rate of diffusion, ω is the rate of advection and k is a rate constant for removal *within* the water column. If there is no removal within the water column (k = 0), the solution to equation [3] for boundary conditions $C(z) = C_0$ at z = 0 (lake surface) and $C(z) = C_m$ at z = m (lake bottom) is:

$$C(z) = C_0 + (C_m - C_0)\frac{e^{\frac{\omega_z}{D_z}z} - 1}{e^{\frac{\omega_z}{D_z}z_m} - 1} \qquad [4]$$

By setting suitable [U] at the top (C_0) and bottom (C_m), model depth profiles can be compared to the data.

The depth profiles for [U] from the different sampling campaigns (Fig. 2,5A) vary between those that are close to continuous U depletion profiles with increasing depth (diffusion-dominated), versus others suggesting a very strong chemocline separating well-mixed upper and lower layers (advection dominated within each layer, diffusion across the chemocline). For example, the entire [U] depth profiles from the early sampling campaigns (e.g. February 2013) can be modelled in terms of processes dominated by diffusion downwards into the sediment (Fig. 5), with no requirement for removal or addition (no reaction term) within the water column. The later sampling campaigns, where a more stratified water column develops,

579 better approximate to two well-mixed reservoirs above and below the chemocline, with more
580 limited mass transfer between (e.g. July 2015; Fig. 5). This type of profile requires advective
581 mixing within the upper and lower layer, coupled to slower diffusive transport across the
582 chemocline, but is also completely consistent with the lack of a removal term within the water
583 column.

584 Overall, then, the first order features for the water-column dissolved pool uranium
585 concentrations require no removal within the water column, consistent with earlier
586 conclusions for the Black Sea and Cariaco Basin that U removal occurs within sulfidic
587 sediments (Anderson, 1987; Anderson et al., 1989a). Further, more detailed, constraints on the
588 U removal process come from water column U isotopes. Uranium isotope fractionation occurs
589 during the U(VI) to U(IV) transition, as evidenced by theoretical equilibrium calculations (e.g.
590 Bigeleisen 1996) and abiotic and biotic experiments (e.g. Basu et al., 2014; Stylo et al., 2015;
591 Stirling et al., 2015; Wang et al., 2015). The overall isotope fractionation associated with
592 uranium reduction is about 1-1.3 ‰, with the heavy isotope preferred in the reduced species
593 (e.g. Bigeleisen, 1996; Fujii et al., 2006; Abe et al., 2008, 2010). In the modern euxinic Black
594 Sea, $\delta^{238}U$ in sediments is generally around 0.4 ‰ higher than the open ocean value, while the
595 deeper water column is driven to lower $\delta^{238}U$ (Weyer et al. 2008; Andersen et al. 2014;
596 Rolison et al. 2017). Previously (Andersen et al. 2014) these data were explained in terms of
597 an effective U isotope fractionation of +0.6‰, i.e. about half the full fractionation, due to U
598 uptake and precipitation in sediments driven by diffusion from overlying seawater and
599 transport-diffusion limitation in the pore water-sediment (e.g. Bender, 1990; Clark and
600 Johnson 2008).

601 If U removal occurs in this manner, the faster removal of ^{238}U than ^{235}U into the sediment
602 should lead to systematically lower $\delta^{238}U$ in the waters above and must occur in a manner that
603 is consistent with the 0.6‰ difference in the sequestration of ^{238}U relative to ^{235}U (see

supplementary text for details). On the other hand, if U were to be removed via reduction in the water column itself with no transport-diffusion limitation, the U isotope fractionation process is expected to produce water column $\delta^{238}U$ values that reflect the full ~1.2 ‰ fractionation. At steady state, the overall input of U and its isotopes to Lake Rogoznica from the open sea must equal the outputs, i.e. outflow of water from the lake to the ocean, and output to sediment:

$$C^{ocean}F_{exch} - C^{lake}F_{exch} - kC^{lake} = 0 \qquad [5]$$

Where C^x is [U] in the ocean or lake, F_{exch} is the water exchange rate and k is a rate constant for removal of U to sediment. Rearranging:

$$C^{lake} = F_{exch}\frac{\left(C^{ocean} - C^{lake}\right)}{k} \qquad [6a]$$

The above is also true for each of ^{238}U and ^{235}U so that:

$$C_{238}^{lake} = F_{exch}\frac{\left(C_{238}^{ocean} - C_{238}^{lake}\right)}{k_{238}} \quad \text{and} \quad C_{235}^{lake} = F_{exch}\frac{\left(C_{235}^{ocean} - C_{235}^{lake}\right)}{k_{235}} \qquad [6b]$$

Combining [6a] and [6b]:

$$\frac{C_{238}^{lake}}{C_{235}^{lake}} = \frac{k_{235}}{k_{238}}\left(\frac{C_{238}^{ocean} - C_{238}^{lake}}{C_{235}^{ocean} - C_{235}^{lake}}\right) \quad [7]$$

Thus, at steady state the average $^{238}U/^{235}U$ ratio of the lake is independent of the relative sizes of the uranium fluxes, and depends only on the isotopic composition of the output to sediment and the degree to which the lake water is modified between input and output.

For Lake Rogoznica, potential scenarios can be examined with the above model of steady state U removal and the $\delta^{238}U$ vs [U] systematics (Fig. 6). The ultimate input of U may be approximated by the open ocean, with $\delta^{238}U$ of -0.4 ‰ and [U] of 13.4 nM. Though this may be slightly modified during transport through the karst, the ($^{234}U/^{238}U$) in the lake water is close to the open ocean value, suggesting this effect is minor. Fig. 6 shows all the water column data for all sampling campaigns. Clearly, though the data lie closer to the diffusion-driven U removal model (solid line in Fig 6A, k_{235}/k_{238} = 0.9994) than one involving irreversible removal in the water column (dashed line in Fig 6A, k_{235}/k_{238} = 0.9988), there is also considerable scatter. Some of this scatter is, however, readily explainable once more in terms of the relative importance of diffusion and advection, with little requirement for reaction within the water column. Thus, for example, data for February 2013 again approximate most closely a situation where diffusion occurs into the sediment across the whole depthscale of the lake (Fig. 6A). But where stratification of the lake occurs, again typified by July 2015 (Fig. 6C), it is only the lower anoxic portion of the lake that approximates the model for diffusion into sediment, whereas the well-mixed upper portion of the lake, now isolated from the sediment by the strong chemocline, shows a more homogeneous U isotopic composition much closer to the oceanic input.

646 The depth profiles for the U isotope data in Fig. 2 clearly point to further minor processes,
647 especially near the chemocline. For example, there is clear but minor isotope exchange with
648 particulate material in July 2013 (Fig. 2) when the dissolved U pool situated just above the
649 chemocline was isotopically light, probably due to the degradation of particulate organic
650 matter with isotopically light U, similar to observed in sediment traps from Saanich Inlet
651 (Holmden et al., 2015). But the above discussion clearly suggests that the first-order process
652 governing U removal at Lake Rogoznica, in common with the Black Sea and despite the
653 higher water column sulfide concentrations, is via U diffusion downward into sediments
654 followed by reductive U precipitation with a net U isotope fractionation of +0.6‰. The
655 dominance of this first–order U removal process should, therefore, be reflected in the
656 authigenic U and its isotope composition imprinted on the sediment.

657

658 ***4.2.2 Mass balance for U and its isotopes in the lake system***

659 In principle, a diffusive removal flux for U can be calculated if the depth of U removal in the
660 pore-waters is known (e.g. Bender, 1990). This estimate could establish whether the U
661 diffusion rate across the sediment-water interface rate is fast enough to account for the
662 observed U accumulation rate in the sediments. However, the pore water data at hand are not
663 at high enough resolution to allow this calculation – the required diffusive flux dictates an e-
664 folding lengthscale for pore water removal of about 0.2 cm. On the other hand, the U isotope
665 composition of the accumulated authigenic U should reflect that dictated by the diffusive U
666 flux model if this represents the main U removal term. Thus, the $^{238}U/^{235}U$ of authigenic U in
667 sediment is expected to be ~0.6‰ heavier than the overlying bottom waters (see
668 supplementary text). At Lake Rogoznica, the average $\delta^{238}U$ of bottom waters for the six
669 sampling campaigns is -0.94±0.07‰ (1SD), while the average authigenic sediment

670 composition is -0.30±0.07‰ (1SD). The difference is in good agreement with the diffusion-
671 driven removal scenario, confirming this process as the main U removal mechanism.

672 In general, if U is to be removed by the U diffusion process from an infinitely large (or
673 rapidly replenished) water column with an open ocean composition (-0.4‰) the $\delta^{238}U$ of
674 authigenic U is expected to be ~+0.2‰. At the other extreme, if the U removal flux is
675 significantly larger than the replenishment rate, thus fully depleting the water column in U,
676 sedimentary authigenic U should equal the input. These systematics reflect the degree of
677 restriction of the system, and are explored in Fig. 7 for Rogoznica and other semi-restricted
678 anoxic basins for which data are available (Kyllaren Fjord, Black Sea, Saanich Inlet, Cariaco
679 Basin, see Table 1). Fig. 7 highlights a clear relationship between the U concentration in the
680 lake bottom waters with the authigenic $\delta^{238}U$ in the sediments (open symbols and blue line).
681 This suggests that the dominant U removal mechanism - U diffusion and reduction within the
682 sediments - was the same in each semi-restricted basin. This includes the Saanich Inlet, in
683 contrast to a previous study (Anderson et al. 1989b) that suggested that the diffusive removal
684 U flux was of insufficient size to be the dominant source of authigenic U in the sediments.
685 However, this latter U removal flux estimate, based on one pore water profile in the anoxic
686 part of the inlet, may have been underestimated due to a lack of representativeness of this one
687 profile or to artifacts during U porewater extraction. A shallow pore water depletion profile of
688 ~0.5 cm (Anderson et al 1989b), similar to that indicated for Lake Rogoznica, would be
689 required for the diffusive U flux to be the dominant U removal process in Saanich Inlet. If the
690 diffusive U flux had indeed been underestimated, this would explain the similarities between
691 authigenic U isotope data in Saanich Inlet sediments (Holmden et al., 2015) and those for
692 other semi-restricted basins, where the diffusive removal process has been shown to be
693 dominant (Figure 7). There is also a reasonably good correlation between authigenic $\delta^{238}U$
694 and water column sulfide concentrations (closed symbols, red line). If U removal is driven by

diffusion into sediment, a mechanistic correlation with the reduction potential of S^- is not expected. But this correlation may be a more-or-less co-incidental consequence of the control that deepwater overturning timescales exert on both sulfide concentrations and authigenic $\delta^{238}U$. Relatively fast water overturning rates would lead to less S^- buildup in the water column, replenishment of U in the water column, and authigenic $\delta^{238}U$ fractionated from open ocean seawater. In contrast, relatively slow deepwater renewal rates may lead to higher S^-, slower U replenishment rates, more quantitative removal of U from the water column and authigenic $\delta^{238}U$ less fractionated from open ocean seawater.

4.3. Mass balance for U, Mo and their isotopes in Lake Rogoznica and other euxinic basins

The impact of deep water renewal rates on sediment geochemistry can be further explored in the context of coupled sedimentary U and Mo concentrations and isotope systematics (Fig. 8). The key difference between Mo and U is the removal mechanism in a euxinic water column, with U driven by diffusion from the water column into sediment where it is fixed, while Mo is scavenged by particulate material in the water column and transported to the sediment in solid form. These different removal mechanisms have been used to fingerprint specific redox conditions using coupled U vs. Mo enrichment systematics in sediment (e.g. Algeo and Tribovillard, 2009). Thus, in a closed system where Mo and U are quantitatively removed, the Mo/U ratio and the Mo and U isotope composition of the sediment should equal the input from the open ocean. Such behaviour is rarely the case, however, with different euxinic basins showing variable Mo/U ratios and Mo and U isotope compositions (Fig. 8). Of the euxinic basins with Mo and U isotope data, only Kyllaren Fjord (Noordmann et al., 2015) shows Mo/U ratios and Mo and U isotope compositions close to the open ocean, indicating near quantitative uptake of both Mo and U. Sediments from the deepest part of the Black Sea

720 (Station 9 with both U and Mo isotope data; Arnold et al., 2004; Andersen et al., 2014) show a
721 Mo/U ratio significantly below the seawater value (see also Tribovillard et al., 2006; Algeo
722 and Tribovillard, 2009). This behaviour has been linked to the contrasting sedimentary output
723 mechanisms for Mo and U, and the fact that the Black Sea exhibits extreme stratification and
724 long deep water renewal times (>500 years; Algeo & Lyons, 2006), leading to deep water Mo
725 depletion from slow resupply (Algeo &Tribovillard, 2009).

726

727 At Lake Rogoznica, Mo/U ratios are, on average, about twice the seawater value (Fig. 8A).
728 Where this has been reported, including at Saanich Inlet (Russell and Morford, 2001;
729 Holmden et al., 2015; Amini et al., 2016) and in the Cariaco Basin (Arnold et al., 2004;
730 Andersen et al., 2014), it is often interpreted as evidence for Mo addition to sediment via a Fe-
731 Mn oxide "particulate shuttle" (e.g. Algeo and Tribovillard, 2009). This suggestion is
732 supported by the previous documentation of isotopically light Mo in such sediments (Fig 8B),
733 and is also consistent with light Mo isotope data at Lake Rogoznica. It is also true, however,
734 that Mo/U ratios higher than seawater are an expected feature of small reservoirs like Lake
735 Rogoznica, even in the absence of a particulate shuttle, because of the more rapid removal of
736 Mo relative to U from the water column to sediment. In fact, any measurement of the basinal
737 average Mo/U ratio of a euxinic setting must record a Mo/U ratio higher than seawater simply
738 because uranium will be lost to a greater extent by flow of water out of the basin than will
739 Mo. For a very small and simple reservoir like Lake Rogoznica, and despite uncertainties such
740 as those arising from the possible operation of a Fe-Mn oxide "particulate shuttle", the
741 different removal rates of Mo and U are likely to give higher Mo/U than that of seawater, and
742 this is likely to be recorded in these sediments. Only in the case where the water flow through
743 the euxinic reservoir is so slow that U diffusion into sediment can keep up, will the Mo/U
744 ratio approach the seawater value. In this context, also implicit in the treatment of Algeo and

745 Tribovillard (2009), the Mo/U ratios lower than seawater in the deep, most sulfidic, portion of
746 the Black Sea only arise because of preferential stripping of Mo relative to U from younger -
747 "upstream" - waters.

748 The Lake Rogoznica isotope data show some similarities to Kyllaren Ford for $\delta^{238}U$, but the
749 low $\delta^{98}Mo$ in both the euxinic waters ($\delta^{98}Mo$ ~2.0-2.4‰) and sediments ($\delta^{98}Mo$ ~1.6-2.2‰),
750 and relatively high Mo/U in the sediments, all seem to require conditions occasionally, though
751 perhaps transient, when isotopically light Mo is added to the basin. The anomalously high
752 [Mo] and low $\delta^{98}Mo$ in April 2013 surface waters, characterised by the lowest $\delta^{98}Mo$ in
753 euxinic waters (~1‰) of any of the sampling campaigns, may have caught one such transient
754 event. However, the arrows on Fig. 8B also indicate schematically how much of the paired
755 Mo-U isotope data for euxinic basins could also be rationalised in terms of (a) variable rates
756 of Mo-U removal relative to each other, possibly driven by variable sulfide concentrations
757 within and between basins, differences in water renewal rates, as well as differences in the
758 ratio of euxinic sediment-water interface (U removal) to volume of euxinic water column (Mo
759 removal); (b) a constant effective $^{238}U/^{235}U$ fractionation factor of about 0.6‰ and; (c) Mo
760 isotope fractionation during the early history of Mo removal, e.g. driven by H_2S
761 concentrations near the action point of switch for complete transformation of $Mo^{VI}O_4^{2-}$ to
762 $Mo^{VI}S_4^{2-}$ (Helz et al., 1996; Tossel et al., 2005; Nägler et al., 2011; Kerl et al., 2017),
763 followed by much more subtle fractionations under the fully euxinic conditions that old
764 waters in the Black Sea encounter (e.g. Nägler et al., 2011). Though the data for sediments
765 recovered beneath the oldest most sulfide-rich waters of the Black Sea support such a
766 scenario, we currently lack paired U-Mo isotope data from sediments deposited from younger
767 waters to fully test this schematic scenario in the Black Sea.

768

769 **5. Conclusions**

770 Data presented in this paper for the temporal variation in the marine Lake Rogoznica, for both
771 Mo and U and their isotopes, has permitted a detailed assessment of the behaviour of these
772 redox-sensitive elements in a small euxinic basin, leading to the following principle
773 conclusions.

774 • Both $\delta^{98}Mo_{part\text{-}diss}$ and $\delta^{98}Mo_{sed\text{-}porewater}$ converge towards a ~0.3‰ offset at high
775 sulfide concentrations, providing further evidence for minor Mo isotope fractionation
776 during non-quantitative Mo uptake into euxinic sediments previously suggested for the
777 Black Sea (Nägler et al. 2011). However, Lake Rogoznica also appears to see periodic
778 addition of significant quantities of isotopically light Mo to the lake waters, possibly
779 from the release of Mo from Fe-Mn oxides formed in the oxic layer.
780
781 • Uranium concentration profiles in the lake waters show clear evidence for a dominant
782 mechanism for removal from solution via U diffusion into, and precipitation within,
783 the euxinic sediments. Periods of more intense stratification lead to well-mixed
784 profiles in the oxic upper and euxinic lower layers, with diffusion across the
785 chemocline only. Furthermore, $\delta^{238}U$ in both the sediments and deep water column are
786 consistent with an effective $^{238}U/^{235}U$ fractionation of +0.6‰ during uptake in the
787 sediments, in line with other studied euxinic basins.
788
789 • As a result of the different uptake mechanisms of U and Mo it is likely that sediments
790 in different areas of a euxinic basin will show different Mo/U, $\delta^{238}U$ and $\delta^{98}Mo$
791 systematics. The exact Mo and U patterns represent an interplay between: (i) the size
792 of the basin; (ii) deep water renewal rates; (iii) water-column sulfide concentrations
793 and; (iv) processes related to the Fe-Mn shuttle. This study further emphasises the

potential of combined Mo and U systematics to provide a better understanding of the redox conditions reflected in the signatures recorded in ancient sediments.

Acknowledgments

This work was supported by ETH Zürich, the Croatian Science Foundation project IP-11-2013-1205, SPHERE and the European Union Seventh Framework Programme (FP7 2007-2013) under grant agreement n° 291823 Marie Curie FP7-PEOPLE-2011-COFUND (The new International Fellowship Mobility Programme for Experienced Researchers in Croatia - NEWFELPRO), as part of the project "Using lakes to develop isotopic tools for understanding ocean redox through Earth history (IsotopicRedoxTools)". GFdS is supported by a Marie Skłodowska-Curie Research Fellowship under EU Horizon2020 (SOSiC; GA #708407). We would like to thank the editor, C. Holmden and two anonymous reviewers for constructive comments on a previous version of the manuscript.

808 **References**

809 Abe, M., Suzuki, T., Fujii, Y., Hada, M., Hirao, K., 2008. An ab initio molecular orbital study
810 of the nuclear volume effects in uranium isotope fractionations. *J. Chem. Phys.***129**,
811 164309.

812 Algeo, T.J. and Lyons, T.W. (2006) Mo-total organic carbon covariation in modern anoxic
813 marine environments: implications for analysis of paleoredox and paleohydrographic
814 conditions. *Paleoceaonography* **21**, 10.1029/2004PA001112.

815 Algeo, T.J. and Tribovillard, N. (2009) Environmental analysis of paleocenographic systems
816 based on molybdenum-uranium covariation. *Chem. Geol*. **268**, 211-225.

817 Amini, M. Weis, D., Soon, M. and Francois, R. (2016) Molybdenum Isotope Fractionation in
818 Saanich Inlet, British Columbia. *Goldschmidt Conference, Yokohama,***60**.

819 Andersen, M., Stirling, C., Zimmermann, B. and Halliday, A. (2010) Precise determination of
820 the open ocean $^{234}U/^{238}U$ composition. *Geochem. Geophys. Geosyst.* **11**,
821 doi.org/10.1029/2010GC003318.

822 Andersen, M.B., Vance, D., Keech, A.R., Rickli, J. and Hudson, G. (2013) Estimating U
823 fluxes in a high-latitude, boreal post-glacial setting using U-series isotopes in soils and
824 rivers. *Chem. Geol.* **354**, 22-32.

825 Andersen, M.B., Romaniello, S., Vance, D., Little, S.H., Herdman, R. and Lyons, T.W.
826 (2014) A modern framework for the interpretation of $^{238}U/^{235}U$ in studies of anciend
827 ocean redox. *Earth Planet. Sci. Lett.* **400**, 184-194.

828 Andersen, M.B., Elliott, T., Freymuth, H., Sims, K.W., Niu, Y. and Kelley, K.A. (2015) The
829 terrestrial uranium isotope cycle. *Nature* **517**, 356-359.

830 Andersen, M.B., Vance, D., Morford, J.L., Bura-Nakić, E., Breitenbach, S.F.M. and Och, L .
831 (2016) Closing in on the marine $^{238}/^{235}U$ budget. *Chem. Geol.* **420**, 11-22.

832 Andersen, M.B., Stirling, C.H. and Weyer, S. (2017) Uranium isotope fractionation. *Reviews*
833 *in Mineralogy & Geochemistry* **82**, 799-850.

834 Anderson, R.F. (1987) Redox behaviour of uranium in an anoxic marine basin. *Uranium* **3**,
835 145-164.

836 Anderson, R.F., Fleischer, M.Q. and LeHurray, A.P. (1989a) Concentration, oxidation state,
837 and particulate flux of uranium in the Black Sea. *Geochim. Cosmochim. Acta* **53**,
838 2215-2224.

839 Anderson, R.F., LeHuray, A.P., Fleisher, M.Q. and Muray, W. (1989b) Uranium deposition in
840 Saanich Inlet sediments, Vancouver Island. Geochim. Cosmochim. Acta **53**, 2202-
841 2213.

842 Archer, C. and Vance, D. (2008) The isotopic signature of the global riverine molybdenum
843 flux and anoxia in the ancient oceans. *Nature Geoscience* **1**, 597-600.

844 Arnold, G.I., Anbar, A.D., Barling, J. and Lyons, T.W. (2004) Molybdenum isotope evidence
845 for widespread anoxia in mid-proterozoic oceans. *Science* **304**, 87-90.

846 Azrieli-Tal, I., Matthews, A., Bar-Matthews, M., Almogi-Labin, A., Vance, D., Archer, C.
847 and Teutsch, N. (2014) Evidence from molybdenum and iron isotopes and
848 molybdenum-uranium covariation for sulphidic bottom waters during Eastern
849 Mediterranean sapropel S1 formation. *Earth Planet. Sci. Lett.* **393**, 231-242.

850 Bargar, J.R., Williams, K.H., Campbell, K.M., Long, P.E., Stubbs, J.E., Suvorova, E.I.,
851 Lezama-Pacheco, J.S., Alessi, P.S., Stylo, M., Webb, S.M., Davis, J.A., Giammar,
852 D.E., Blue, L.Y. and Bernier-Latmani, R. (2013) Uranium redox transformation
853 pathways in acetate-amended sediments. *Proc. Natl. Acad. Sci. U.S.A.* **110(12)**, 4506-
854 4511.

855 Barling, J., Arnold, G.L. and Anbar, A.D. (2001) Natural mass-dependent variations in the
856 isotopic composition of molybdenum. *Earth Planet. Sci. Lett.* **193**, 447-457.

857 Barling, J. and Anbar, A.D. (2004) Molybdenum isotope fractionation during adsorption by
858 manganese oxides. *Earth Planet. Sci. Lett.* **217**, 315-329.

859 Barnes, C.E, and Cochran, J.K. (1990) Uranium removal in oceanic sediments and the
860 oceanic-U balance. *Earth Planet. Sci. Lett.* **97**, 94-101.

861 Basu, A., Stanford, R.A., Johnson, T.M ., Lundstrom, C.C . and Löfller, F.E. (2014) Uranium
862 isotopic fractionation factors during U(VI) reduction by bacterial isolates. *Geochim.*
863 *Cosmochim. Acta* **136**, 100-113.

864 Bender, M.L. (1990) The $\delta^{18}O$ of dissolved O_2 in seawater: a unique tracer of circulation and
865 respiration in the deep sea. *J. Geophys. Res., Oceans* **95**, 22242-22252.

866 Bigeleisen, J. (1996) Nuclear size and shape effects in chemical reactions. Isotope chemistry of heavy
867 elements. *J. Amer. Chem. Soc.* **118**, 3676-3680.

868 Bostick, B.C., Fendore, S. and Helz, G.R. (2003) Differential adsorption of molybdate and
869 tetrathiomolybdate on pyrite (FeS_2). *Environ. Sci. Technol.* **37**, 285-291.

870 Brennecka, G.A., Herrmann, A.D., Alego, T.J. and Anbar, A.D. (2011a) Rapid expansion of
871 oceanic anoxia immediately before the end-Permian mass extinction. *Proc. Natl. Acad.*
872 *Sci.* **108**, 17631-17634.

873 Brennecka, G.A., Wasylenki, L.E., Bargar, J.R., Weyer, S. and Anbar, A.D. (2011b) Uranium
874 isotope fractionation during adsorption to Mn-oxyhydroxides. *Environ. Sci. Technol.*
875 **45**,1370-1375.

876 Bura-Nakić, E., Helz, G.R., Ćosović, B. and Ciglenečki, I. (2009) Reduced sulfur species in a
877 stratified seawater lake (Rogoznica Lake, Croatia); seasonal variations and evidence
878 for organic carriers of reactive sulfur. *Geochim. Cosmochim. Acta* **73**, 3738–3751.

879 Cheng, H., Edwards, R.L., Sehe, C.C ., Polyak, V.J., Asmerom, Y., Woodhead, Y.,
880 Hellstrom, J., Wang, Y., Kong, X., Spötl, C., Wang, X. and Alexander Jr., C. (2013)
881 Improvements in ^{230}Th dating, ^{230}Th and ^{234}U half-life values, and U-Th isotopic
882 measurements by multi-collector inductively couples plasma mass spectrometry. *Earth*
883 *Planet. Sci. Lett.* **371-372**, 82-91.

884 Ciglenečki, I., Janeković, I., Marguš, M., Bura-Nakić, E., Carić, M., Ljubešić, Z., Batistić, M.,
885 Hrustić, E., Dupčić, I. and Garić, R. (2015) Impacts of extreme weather events on
886 higly eutrophic marine ecosystem (Rogoznica Lake, Adriatic coast). *Cont. Shelf Res.*
887 1**08**, 144-155.

888 Ciglenečki, I., Carić, M., Kršinić, F., Viličić, D. and Ćosović, B. (2005) The extintion by
889 sulfide - turnover and recovery of a naturally eutrophic, meromictic seawater lake. *J.*
890 *Mar. Sys*. **56**, 29-44.

891 Clark, S.K. and Johnson, T.M. (2008) Effective isotopic fractionation factors for solute
892 removal by reactive sediments: a laboratory microcosm and slurry study. *Environ. Sci.*
893 *Technol.* **42**, 7850-7855.

894 Collier, R.W. (1985) Molybdenum in the Northeast Pacific Ocean. *Limnol. Oceanogr.* **30**,
895 1351-1354.

896 Colodner, D., Edmond, J. and Boyle, E. (1995) Rhenium in the Black Sea: comparison with
897 molybdenum and uranium. *Earth Planet. Sci. Lett.* **131**, 1-15.

898 Dahl, T.W., Anbar, A.D., Gordon, G.W., Rosing, M.T., Frei, R. and Canfield, D.E. (2010)
899 The behavior of molybdenum and its isotopes across the chemocline and in the

900 sediments of sulfidic Lake Cadagno, Switzerland. *Geochim. Cosmochim. Acta* **74**,
901 144-163.

902 Emerson, S.R. and Huested, S.S. (1991) Ocean anoxic and the concentration of molybdenum
903 and vanadium in seawater. *Mar. Chem*. 3**4**, 177-196.

904 Erickson, B.E., and Helz, G.R. (2000) Molybdenum (VI) speciation in sulphidic waters:
905 stabiity and lability of thiomolybdates. *Geochim. Cosmochim. Acta* **64**, 1149-1158.

906 Goldberg, T., Archer, C., Vance, D. and Poulton, S.W. (2009) Mo isotope fractionation during
907 adsorption to Fe (oxyhydr)oxides. *Geochim. Cosmochim. Acta* **73**, 6502-6516.

908 Fujii, Y., Higuchi, N., Haruno, Y., Nomura, M. and Suzuki, T. (2006) Temperature
909 dependence of isotope effects in uranium chemical exchange reactions. *J. Nucl. Sci.*
910 *Technol.* **43**, 400–406.

911 Gordon, G.W., Lyons, T.W., Arnold, G.L., Roe, J., Sageman, B.B. and Anbar, A.D. (2009)
912 When do black shales tell molybdenum isotope tales? *Geology* **37**, 535-538.

913 Helz, G.R., Miller, C.V., Charnock, J.M., Mosselmans, J.F.W., Pattrick, R.A.D., Garner, C.D.
914 and Vaughan, D.J. (1996) Mehanism of molybdenum removal from the sea and its
915 concentration in black shales: EXAFS evidence. *Geochim. Cosmochim. Acta* **60**, 3631-
916 3642.

917 Helz, G.R., Bura-Nakić, E., Mikac, N. and Ciglenečki, I. (2011) New model for molybdenum
918 behavior in euxinic waters. *Chem. Geol*. **284**, 323-332.

919

920 Herrmann, A.D., Kendall, B., Alego, T.J., Gordon, G.W., Wasylenki, L.E., and Anbar, A.D.
921 (2012) Anomalous molybdenum isotope trends in Upper Pennsylvanian euxinic facies:
922 Significance for use of ^{98}Mo as a global marine redox proxy. *Chem. Geol*. **324-325**,
923 87-98.

924 Hinojosa, J.L., Stirling, C.H., Reid, M.R., Moy, C.M. and Wilson, G.S. (2016) Trace metal
925 cycling and $^{238}U/^{235}U$ in New Zealand's fjords: Implications for reconstructing global
926 paleoredox conditions in organic-rich sediments. *Geochim. Cosmocim. Acta* **179**, 89-
927 109.

928 Holmden, C., Amini, M. and Francois, R. (2015) Uranium isotope fractionation in Saanich
929 Inlet: A modern analog study of a paleoredox tracer. *Geochim. Cosmochim. Acta* **153**,
930 202-215.

931 Kerl, C.F., Lohmayer, R., Bura-Nakić, E., Vance, D. and Planer-Friedrich, B. (2017)
932 Experimental confirmation of isotope fractionation in thiomolybdates using ion
933 chromatography and detection by multi-collector ICP-MS. *Anal. Chem.* **89**, 3123-
934 3129.

935 Klinkhammer, G.P. and Palmer, M.R. (1991) Uranium in the oceans: where it goes and why.
936 *Geochim. Cosmochim. Acta* **55**, 1799-1806.

937 Kowalski, et al. (2013): Pelagic molybdenum concentration anomalies and the impact of
938 sediment resuspension on the molybdenum budget in two tidal systems of the North
939 Sea. Geochim. Cosmochim. Acta, 119, 198-211. dx.doi.org/10.1016/j.gca.2013.05.046

940
941 Ku, T.L., Knauss, K.G. and Mathieu, G.G. (1977) Uranium in open ocean: concentration and
942 isotopic composition. *Deep-Sea Res.* **24**, 1005-1017.McLennan, S.M. (2001)
943 Relationships between the trace element composition of sedimentary rocks and upper
944 continental crust. *Geochem.Geophys. Geosyst.* **2**, doi: 10.1029/2000GC000109.

945 Lovley, D.R., Phillips, E.J.P., Gorby, Y.A., Landa, E.R., 1991. Microbial Reduction of
946 Uranium. Nature 350, 413-416McManus, et al. (2002): Oceanic molybdenum isotope
947 fractionation: Diagenesis and hydrothermal ridge-flank alteration. Geochemistry,
948 Geophysics, Geosystems, 3 (12), 1078,doi:10.1029/2002GC000356,2002.

McManus, J., Berelson, W.M., Klinkhammer, G.P., Hammond, D.E. and Holm, C. (2005) Authigenic uranium: relationship to oxygen penetration depth and organic carbon rain. *Geochim. Cosmochim. Acta* **69**, 95-108.

McManus, J., Berelson, W.M., Severmann, S., Poulson, R.I., Hammond, D.E., Klinkhammer, G.P. and Holm, C. (2006) Molybdenum and uranium geochemistry in continental margin sediments: paleoproxy potential. *Geochim. Cosmochim. Acta* **70**, 4643-4662.

Millero, F.J. (1986) The thermodynamic and kinetics of the hydroge sulfide system in natural waters. *Mar. Chem.* **18**, 121-147.

Montoya-Pino, C,, Weyer, S., Anbar, A.D.,Pross, J., Oschmann, W., van de Schootbruuge, B. and Arz, H.W (2010) Global enhancment of ocean anoxia during Anoxic Oceanic Event 2: A quantitative approach using U isotopes. *Geology* **38**, 315-318.

Morford, J.L. and Emerson, S. (1999) The geochemistry of redox sensitive trace metals in sediments. *Geochim. Cosmochim. Acta* **63**, 1735-1750.

Nägler, T.F., Neubert, N., Böttcher, M.E., Dellwig, O. and Schnetger,B. (2011) Molybdenum isotope fractionation in pelagic euxinia: Evidence from the modern Black and Baltic Seas. *Chem. Geol*. **289**, 1-11.

Nägler, T.F., Anbar, A.D., Archer, C., Goldberg, T., Gordon, G.W., Greber, N.D., Siebert, C., Sohrin, Y. and Vance, D. (2014) Proposal for an international molybdenum isotope measurement standard and data representation. *Geostand. Geoanal. Res.* **38**, 149-151.

Nakagawa, Y., Takano, S., Firdaus, M.L., Norisuye, K., Hirata, T., Vance, D. and Sohrin, Y. (2012) The molybdenum isotopic composition of the modern ocean. *Geochem. J.* **46**, 131-141.

Noordmann, J., Weyer, S., Montoya-Pino, C., Dellwig, O., Neubert, N. and Eckert, S. (2015) Uranium and molybdenum isotope systematics in modern euxinic basins: Case studies

973 from the central Baltic Sea and the Kyllaren fjord (Norway). *Chem. Geol*. **396**, 182-
974 195.

975 Poulson, R.L., Siebert, C., McManus, J., Severmann, S. and Berelson, W.M. (2006)
976 Authigenic molybdenum isotopes signatures in marine sediments. *Geology*, **34**, 617-
977 620.

978 Poulson Brucker, R.L., McManus, J., Severmann, S. and Berelson, W.M. (2009)
979 Molybdenum behavior during early diagenesis: insights from Mo isotopes. *Geochem.*
980 *Geophy. Geosyst.* **10**, doi:10.1029/2008GC002180.

981 Prospero, J. M. (1996). Saharan dust transport over the North Atlantic Ocean and
982 Mediterranean: an overview. In *The impact of desert dust across the Mediterranean*
983 (eds. Guerzoni, S. and Chester R.). Netherlands, Springer, pp. 133-151.

984 Richter, S., Alonso-Munoz, A., Eykens, R., Jacobsson, U., Kuehn, H., Verbruggen, A.,
985 Aregbe, Y., Wellum, R. and Keegan, E. (2008). The isotopic composition of natural
986 uranium samples-Measurements using the new n(^{233}U)/n(^{236}U) dobule spike IRMM-
987 3636. *Int. J. Mass Spectrom.* **269**, 146-148.

988 Rolison, J.M., Stirling, C.H., Middag, R. and Rijkenberg, M. J.A. (2017) Uranium stable
989 isotope fractionation in the Black Sea: modern calibration of the ^{238}U/^{235}U paleo-redox
990 proxy. *Geochim. Cosmochim. Acta* **203**, 69-88.

991 Russell, A.D. and Morford, J.L. (2001) The behaviour of redox-sensitive metals across a
992 laminated - massive-laminated transition in Saanich Inlet, British Columbia. *Marine*
993 *Geology*. **174**, 341-354.

994 Scheiderich, K., Zerkle, A.L., Helz, G.R., Farquhar, J. and Walker, R.J. (2010) Molybdenum
995 isotope, multiple sulfur isotope, and redox sensitive elementa behavior in early
996 Pleistocene Mediterranean Sapropels. *Chem. Geo*l. **279**, 134-144.

997 Scott, C., Lyons, T.W., Bekker, A., Shen, Y., Poulton, S.W., Chu, X. and Anbar, A.D. (2008)
998 Tracing the stepwise oxygenation of the Proterozoic ocean. *Nature* **452**, 456-459.

999 Siebert, C., Nägler, T.F., von Blanckenburg, F. and Kramers, J.D. (2003) Molybdenum
1000 isotope records as a potential new proxy for paleocenography. *Earth Planet. Sci. Lett.*
1001 **211**, 159-171.

1002 Siebert, C., McManus, J., Bice, A., Poulson, R. and Berelson, W.M. (2006) Molybdenum
1003 isotope signatures in continental margin marine sediments. *Earth Planet. Sci. Lett.*
1004 **241**, 723-733.

1005 Stirling, C.H., Andersen, M.B., Potter, E.K. and Halliday, A.N. (2007) Low temperature
1006 isotopic fractionation of uranium. *Earth Planet. Sci. Lett.* **264**, 208-225.

1007 Stirling, C.H., Andersen, M.B., Warthmann, R. and Halliday, A.N. (2015) Isotope
1008 fractionation of ^{238}U and ^{235}U during biologically-mediated uraium reduction.
1009 *Geochim. Cosmochim. Acta* **163**, 200-218.

1010 Stylo, M., Neubert, N., Wang, Y., Monga, N., Romaniello, S.J. and Weyer, S. (2015)
1011 Uranium isotopes fingerprint biotic reduction. *Proc. Natl. Acad. Sci.* **112**, 5619-5624.

1012 Taylor, R.N. and McLennan, S. (1985) *The Continental Crust: Its Composition and Evolution.*
1013 Blackwell, Boston.

1014 Tissot, F.L.H. and Dauphas, N. (2015) Uranium isotopic compositions of the crust and ocean:
1015 age corrections, U budget and global extent of modern anoxia. *Geochim. Cosmochim.*
1016 *Acta* **167**,113-143.

1017 Tossell, J.A. (2005) Calculating the partitioning of the isotopes of Mo between oxidic and
1018 sulfidic species in aqueous solution. *Geochim. Cosmochim. Acta* **69**, 2981-2993.

1019 Tribovillard, N., Alego, T., Lyons, T.W. and Riboulleau, A. (2006) Trace metals as
1020 paleoredox and paleoproductivity proxies: an update. *Chem. Geol.* **232**, 12-32.

1021 Tribovillard, N., Alego, T.J., Baudin, F. and Riboulleau, A. (2012) Analysis of marine
1022 environmental conditions based on molybdenum - uranium covariation - Applications
1023 to Mesozoic paleocenography. *Chem. Geol*. **324-325**, 46-58.

1024 Vogelin, A.R., Nägler, T.F., Samankassou, E. and Villa, I.M. (2009) Molybdenum isotopic
1025 composition of modern and Carboniferous carbonates. *Chem. Geol*. **265**, 488-498.

1026 Vogelin, R.A., Nägler, T.F., Beukes, N.J. and Lacassie, J.P. (2010) Molybdenum isotopes in
1027 late Archean carbonate rocks: Implications for early Earth oxygenation. *Precambrian*
1028 *Res.* **182**, 70-82.

1029 Vogelin, A.R., Pettke, T., Greber, N.D., von Niderhäusen, B. and Nägler, T. (2014) Magma
1030 differentiation fractionates Mo isotopes ratios: evidence from the Kos Plateau Tuff
1031 (Aegean Arc). *Lithos* **190-191**, 440-448.

1032 Vorlicek, T.P., and Helz, G.R. (2002) Catalysis by mineral surfaces: implications for Mo
1033 geochemistry in anoxic environments. *Geochim. Cosmochim. Acta* **66**, 3679-3692.

1034 Wang, X., Johnson, T.M. and Lundstrom, C.C., 2015. Isotope fractionation during oxidation
1035 of tetravalent uranium by dissolved oxygen. *Geochim. Cosmochim. Acta* **150**, 160–
1036 170.

1037 Westermann, S., Vance, D., Cameron, V., Archer, C. and Robinson, S.A. (2014)
1038 Heterogeneous oxidation states in the Atlantic and Tethys oceans during Oceanic
1039 Anoxic Event 2. *Earth Planet. Sci. Lett.* **404**, 178-189.

1040 Weyer, S., Anbar, A.D., Gerdes, A., Gordon, G.W., Alego, T.J. and Boyle, E.A. (2008)
1041 Natural fractionation of $^{238}U/^{235}U$. *Geochim. Cosmochim. Acta* **72**, 345-359.

1042 Zheng, Y., Anderson, R.F., van Geen, A., Fleischer, M.Q., 2002. Preservation of particulate
1043 non-lithogenic uranium in marine sediments. Geochimica et Cosmochimica Acta 66,
1044 3085-309
1045

Figure captions

Figure 1: Depth–time sections for salinity, oxygen, sulfide, and particulate Fe and Mn concentrations in Lake Rogoznica during 2013 (February, April, July and October) and 2015 (April and July).

Figure 2: Depth profiles of dissolved (salinity normalised) and particulate Mo and U concentrations, dissolved and particulate $\delta^{98}Mo$ and $\delta^{238}U$. The very high Mo concentration at the surface (0 m) in April and July 2013, as well as the low $\delta^{238}U$ in July 2013 (7.5 m), are given as numerical values.

Figure 3: Authigenic sedimentary and pore water Mo and U concentrations, as well as $\delta^{98}Mo$ and $\delta^{238}U$, in the sediment core recovered from the anoxic portion of Lake Rogoznica, plotted versus depth beneath the sediment water interface. The dashed lines on all four plots show the isotopic composition of the open ocean for Mo and U.

Figure 4: A: Mo isotopic composition plotted against reciprocal Mo concentration for all samples with O_2 > 5mg l^{-1}. Most data fall along a flat trajectory close to oceanic Mo isotope ratios at variable Mo concentrations (horizontal grey arrow). Some data for April and July 2013, however, show higher Mo concentrations and lower $\delta^{98}Mo$, lying along a trajectory that requires an extra source of Mo with $\delta^{98}Mo$ around +0.4 to +0.5‰. B: $\delta^{98}Mo_{diss\text{-}part}$ for all dissolved-particulate pairs, including sediment-pore water, for samples where sulfide is detectable. The water column data appear to become asymptotic to a value around +0.3‰ at very high dissolved sulfide concentrations. Though pore water data are more scattered, no $\delta^{98}Mo_{diss\text{-}part}$ is below this value.

Figure 5: A: Salinity-normalised [U] data from the February 2013 campaign (red diamonds); the modelled thick black line on the diagram is for a virtually stagnant lake (no advection) in which U diffuses downwards into the sediment. The relative importance of advection versus

diffusion is represented by the value of ω/D, which is ~0.007 for the modelled evolution. For comparison, the thin dashed line shows a profile dominated by advection, with a ω/D = 0.7, two orders of magnitude greater. B: All data from the four intermediate sampling campaigns. C: Data from the July 2015 campaign (purple circles). The water column is separated into two rather isolated layers above and below the chemocline. The black curve shows the impact of transport within each layer that is completely dominated by advection over diffusion (ω/D = 2±0.3) - both reservoirs are well mixed for [U] with much slower communication across the chemocline.

Figure 6: Salinity-normalised [U] vs. $\delta^{238}U$ for Lake Rogoznica. A: Data from the February 2013 campaign (red diamonds), which, as for [U] (Fig 5), most closely follow the expected trajectory for diffusion-driven U removal from a stagnant water column. The red dotted line is a regression of the data (based on 1/[U] vs $\delta^{238}U$). The curved solid black line shows the approximate trajectory expected for the waters, with diffusion-driven U removal with a +0.6‰ difference in the removal rate constants for ^{238}U and ^{235}U, and a starting composition similar to water sample with the highest [U] (see supplementary text for details). The dashed line shows the trajectory for removal within the water column via a Rayleigh process with a 1.2‰ fractionation in $^{238}U/^{235}U$, starting from the same water sample as the diffusion model. B: All data from the four intermediate sampling campaigns. C: Data for July 2015 (purple circles) which, again like the [U] data (Fig 5), show strong asymmetry. This profile is characterised by an upper oxic layer that is near homogeneous in [U] and $\delta^{238}U$ because of isolation from the sediment by a strong chemocline, and a lower anoxic layer. The [U]-$\delta^{238}U$ systematics in the lower anoxic layer (1/[U] vs $\delta^{238}U$ regression; dotted line) follow the model trajectory for diffusion-driven U removal from a stagnant water column (solid line), with the deepest oxic sample, nearest the chemocline, used as the upper boundary for both the regression line and diffusion modelling.

Figure 7: Relationship between $\delta^{238}U_{auth}$ and (i) the percentage of dissolved U removal in deep anoxic vs surface water (bottom axis, open symbols, blue regression line) and (ii) total dissolved sulfide (ΣS^{2-}) in the anoxic part of the water column (closed symbols, red regression line). Sulfide concentrations in Supplementary Table 2. See Table 1 for citations to data. The slope of the U removal vs. $\delta^{238}U_{auth}$ best fit regression line is close to that expected for diffusive removal U flux with an effective $^{238}U/^{235}U$ fractionation ~+0.6 (see supplementary text).

Figure 8: A: U vs Mo enrichment factors and, B: authigenic $\delta^{98}Mo$ vs. $\delta^{238}U$, for Lake Rogoznica sediments (individual sediment horizons, open circles; average, filled circle) compared to other euxinic basins. Key to colours for both panels as indicated in Panel B. Data sources: Kyllaren Fjord (Noordmann et al., 2015), Black Sea (Station 9 data in Arnold et al., 2004; Andersen et al., 2014), Cariaco Basin (Arnold et al., 2004; Andersen et al., 2014), Saanich Inlet (Russell and Morford, 2001; Holmden et al., 2015; Amini et al., 2016). In A the seawater Mo/U is plotted as the solid line, with deviations from the seawater ratio shown as dashed lines as indicated. In B schematic solid arrows show how sediment deposited beneath euxinic waters would vary in different euxinic basins for high versus low rates of Mo removal relative to U, assuming a constant fractionation factor for uranium isotopes. These scenarios would require Mo fractionation during initial non-quantitative removal to be substantial, but more subtle during the subsequent more quantitative removal, consistent with theoretical, experimental and observational constraints (e.g. Helz et al., 1996; Tossel, 2005; Nägler et al., 2011; Kerl et al., 2017).

1121
1122

1123 **Table 1:** $[\Sigma S^{-II}]$, $[U]_{diss}$ and $\delta^{238}U$ of dissolved ($\delta^{238}U_{diss}$) and authigenic sedimentary ($\delta^{238}U_{auth}$)
1124 uranium in the anoxic water columns and sediments of different modern anoxic basins.

Euxinic basin	Salinity norm. $[U]_{diss}$ nmol l^{-1} **	$\delta^{238}U_{auth}$ in sediments	$\delta^{238}U_{diss}$ deep waters	$[\Sigma S^{-II}]$ µmol l^{-1} deep waters	Source
Lake Rogoznica*	2.8/***	-0.30	-0.94	1214	This work
Kyllaren Fjord	7.5/12.9	-0.22	-0.71	4316	Noordmann et al. (2015)
Black Sea	9.3/17.3	-0.03	-0.68	262	Rolison et al. (2016)
Cariaco Trench	12.0/14.5	+0.03	-	40	Anderson (1987) Emerson and Huested (1991) Andersen et al. (2014)
Saanich Inlet	14.7/15.4	+0.17	-0.48	30	Emerson and Huested (1991) Holmden et al. (2015)

1125 *average values for $[U]_{diss.}$, $\delta^{238}U_{auth}$, $\delta^{238}U_{diss.}$ and ΣS^{-II} in the deepest anoxic Lake Rogoznica samples from all 6
1126 sampling events.
1127 *Salinity normalised (35) U concentrations for deep waters/surface waters. This ratio is used for the U water
1128 column removal fraction in Figure 7.
1129 ***A [U] as the open ocean was used for the surface waters (13.4 $nmol^{-1}$) in this setting.
1130
1131

1132

Figure 1

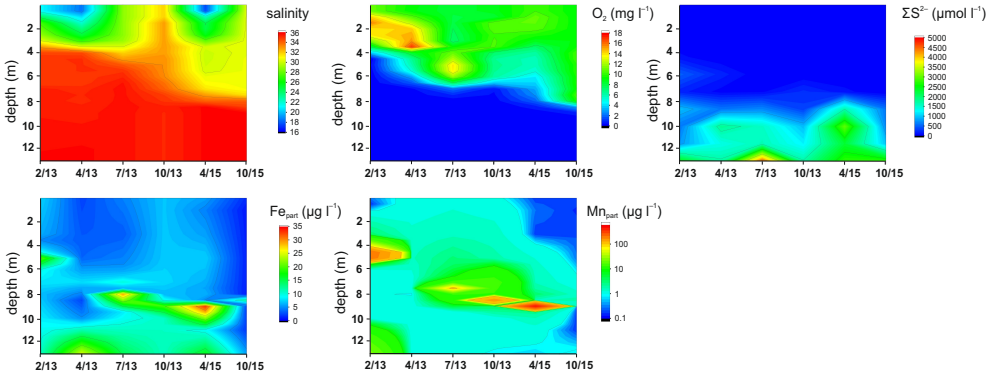

1133
1134

1135

Figure 2

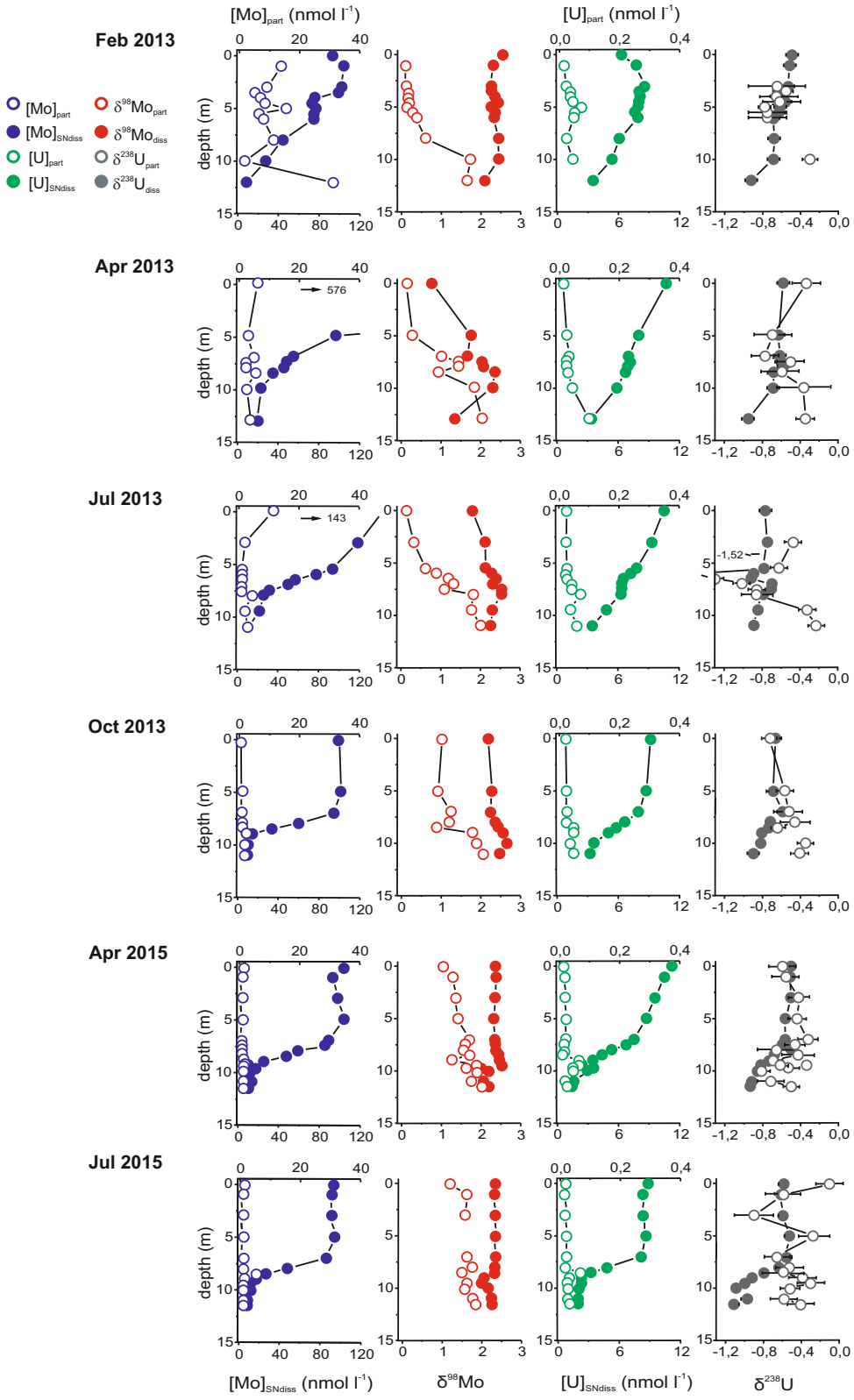
[Mo]part (nmol l-1)
[U]part (nmol l-1)
Feb 2013
Apr 2013
Jul 2013
Oct 2013
Apr 2015
Jul 2015
[Mo]part
[Mo]SNdiss
[U]part
[U]SNdiss
δ98Mopart
δ98Modiss
δ238Upart
δ238Udiss
depth (m)
576
143
-1,52
[Mo]SNdiss (nmol l-1)
δ98Mo
[U]SNdiss (nmol l-1)
δ238U

1140

Figure 3

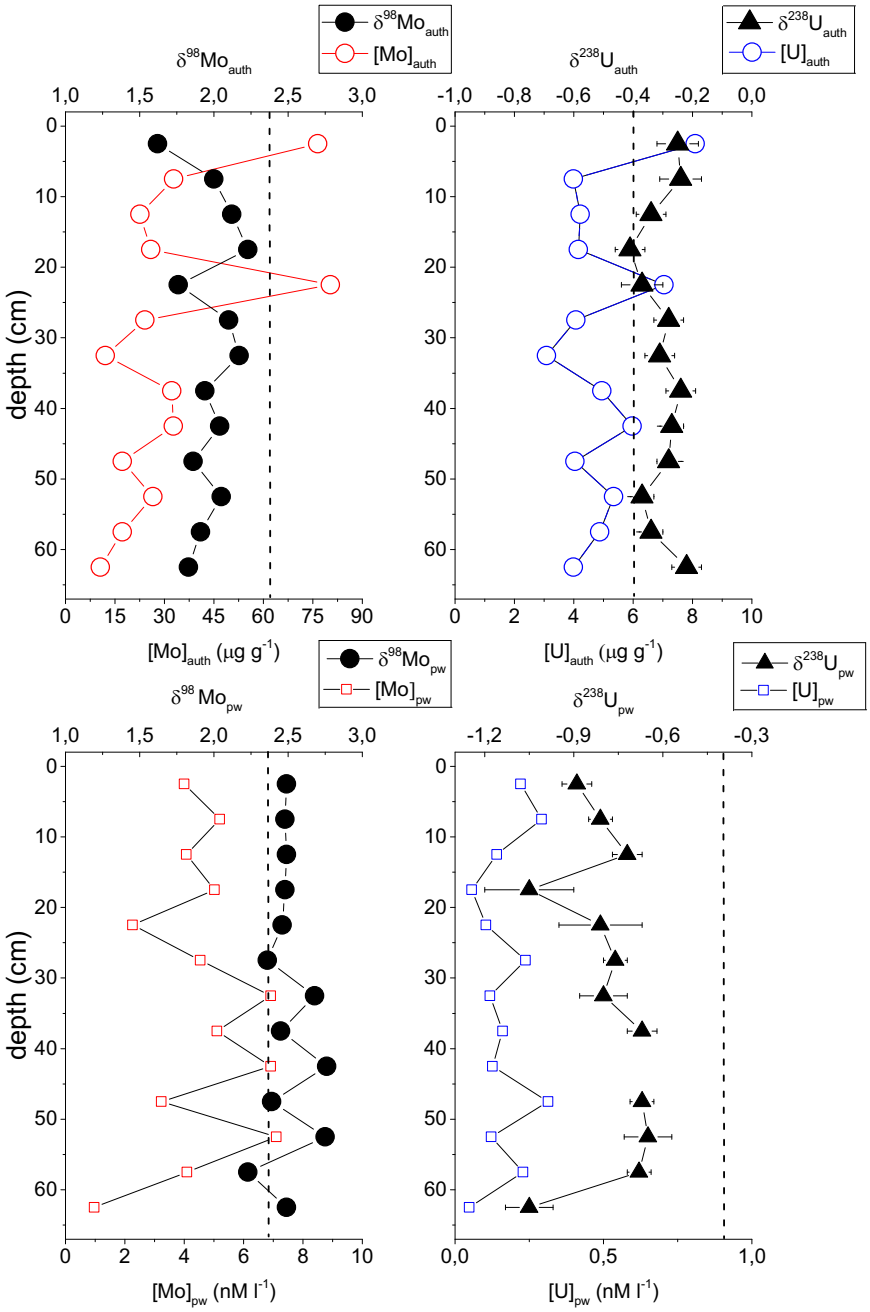

1141

1142

1143

1144

Figure 4

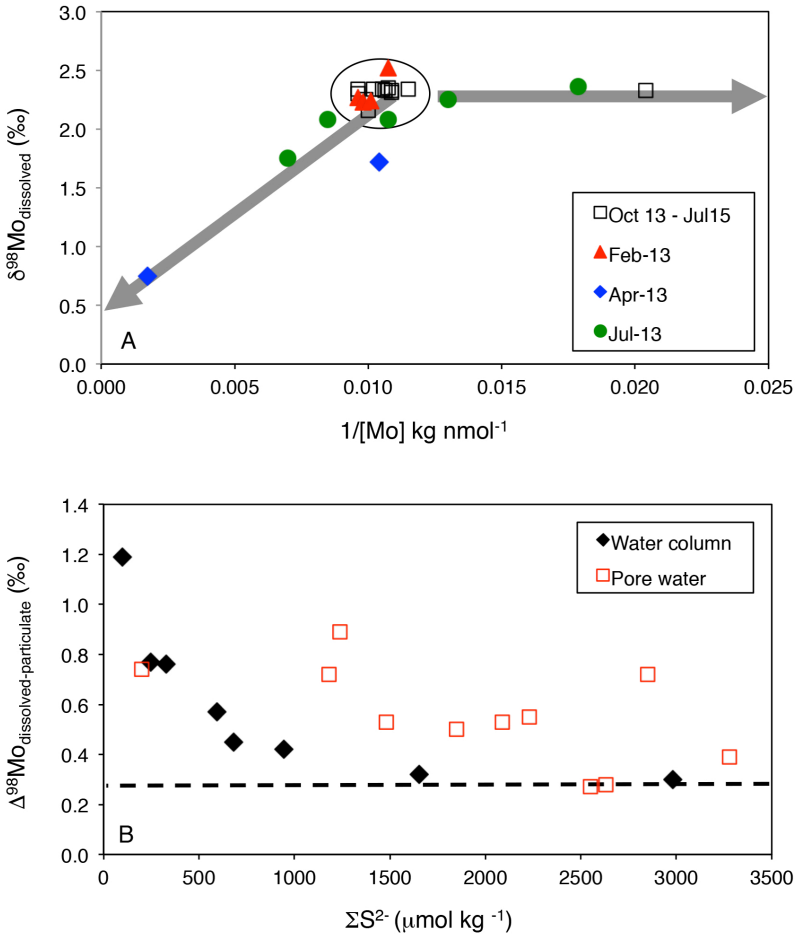

1145

1146

1147

1148

Figure 5

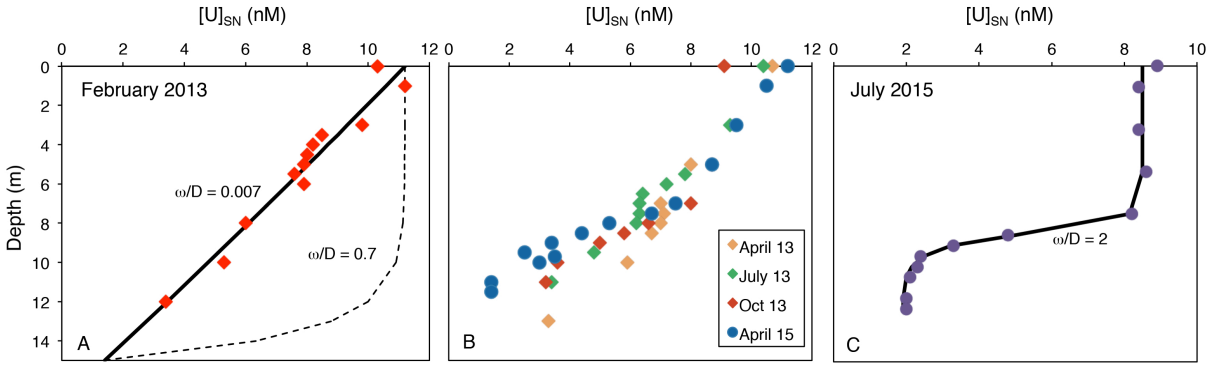

1149

1150

1151 **Figure 6**

1152

1153

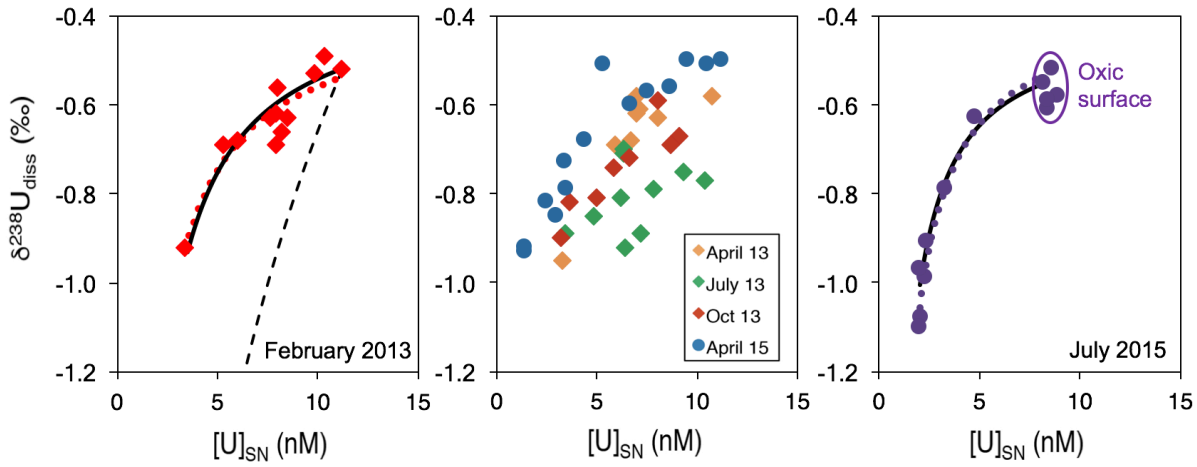

1154

1155

1156 **Figure 7**

1157

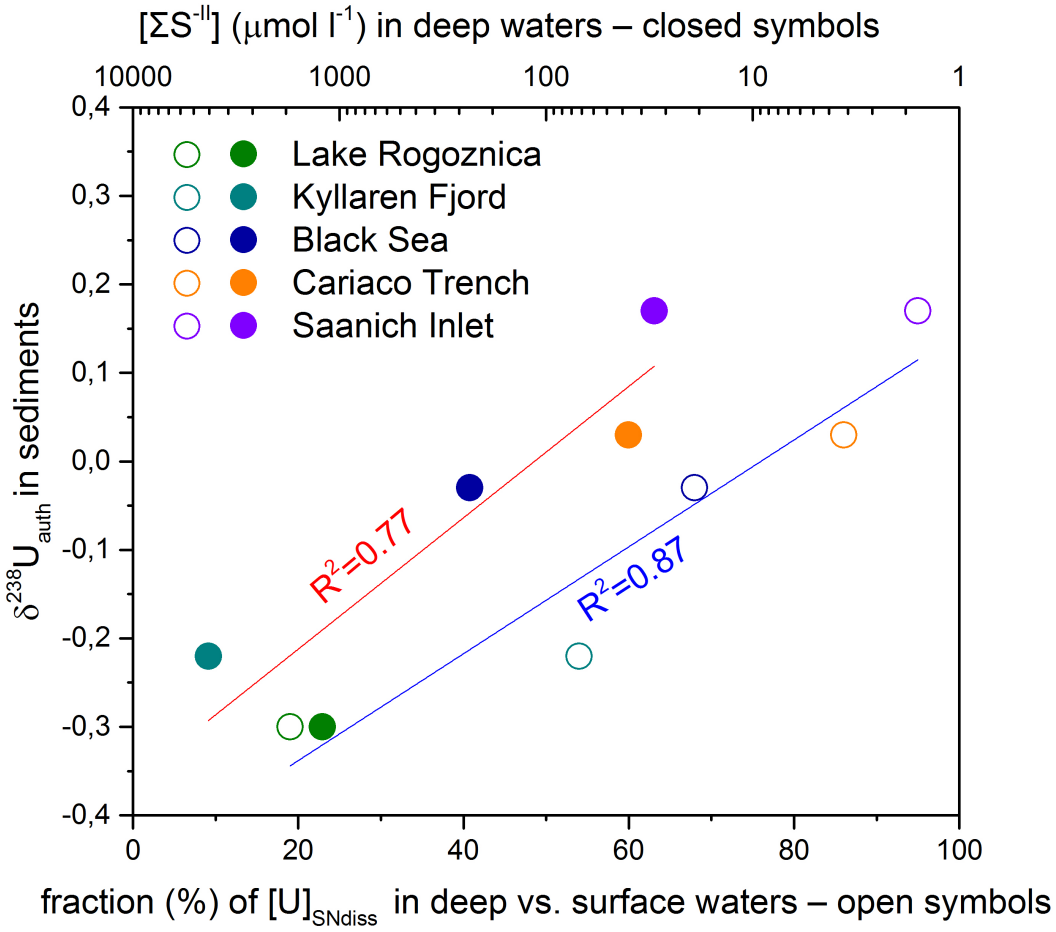

1158

1159

1160

1161

1162

Figure 8

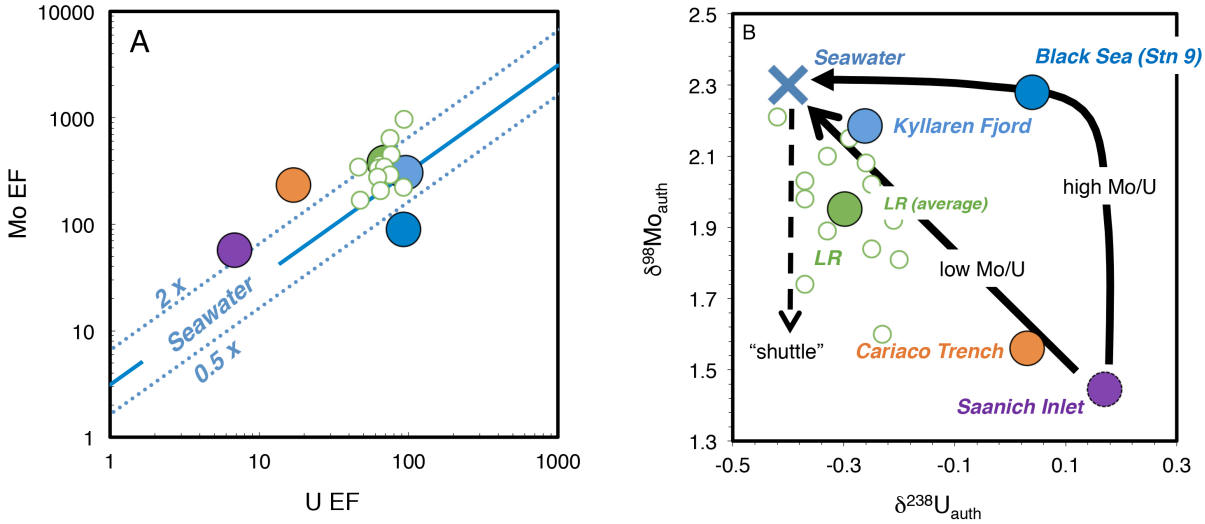
A
Mo EF
U EF
10000
1000
100
10
1
1
10
100
1000
2 x
Seawater
0.5 x
B
$\delta^{98}Mo_{auth}$
$\delta^{238}U_{auth}$
2.5
2.3
2.1
1.9
1.7
1.5
1.3
-0.5
-0.3
-0.1
0.1
0.3
Seawater
Black Sea (Stn 9)
Kyllaren Fjord
high Mo/U
LR (average)
LR
low Mo/U
"shuttle"
Cariaco Trench
Saanich Inlet

Supplementary text to 'Coupled Mo-U abundances and isotopes in a small marine euxinic basin: constraints on processes in euxinic basins' by Bura-Nakic et al.

We constructed a simple one-dimensional water-column model in order to assess the covariation between [U] and $\delta^{238}U$ expected, when U is only removed from the very bottom of the water column (by diffusion into sediment) with an effective isotope effect of +0.6‰. For simplicity, the model only considers the well-mixed portion of the water column above the sediments, such that we need only consider non-directional mixing processes within the water column and can ignore unidirectional advective transport. We do this by discretizing the water column into a series of 0.1m-high cells, each of which exchanges a constant volume flux (ν) with its immediate neighbours. Uranium is transported conservatively within the water column, and lost only from the lowermost cell of the simulated water column. The model carries tracers of ^{235}U and ^{238}U, and the isotope fractionation associated with loss to sediments is represented as a differential first-order rate constant (k) for these two tracers.

Our model can be applied to the entire 15m depth of Lake Rogoznica in February 2013, when [U] decreases near-linearly with depth and can be well described by a water column dominated by diffusion (see Section 4.2.1 and Fig. 5 of the main text). In order to compare the model result to the data, the surface boundary condition of the model is initialised with [U] and $\delta^{238}U$ values observed at the top of the water column in February 2013. The simulated [U] and $\delta^{238}U$ profiles depend on the ratio of the exchange flux ν to the loss rate-constant k. We set this ratio so as to reproduce the observed [U] gradient in February 2013 (Fig. S1); the model simulates the corresponding $\delta^{238}U$ profile expected when U is lost from the very bottom of the water column with an isotope effect of +0.6‰. As can be seen in Fig. S1, (and Fig. 6A of the main manuscript), the model reproduces the observed co-variation between [U] and $\delta^{238}U$. Interestingly, the simulated co-variation is essentially identical to the mixing trend predicted by linear regression of $\delta^{238}U$ against 1/[U] (blue line in Fig. S1). Simulating U-loss to sediment with an isotope effect of +0.6‰ is thus sufficient to reproduce the degree of $\delta^{238}U$ variation and observed co-variation between [U] and $\delta^{238}U$. It is important to reiterate that the model result is independent of the numerical values of ν and k, being instead controlled by the ratio between them, which sets the [U] gradient across the water column.

More generally, the model can be applied to study the U isotope systematics of well-mixed euxinic water columns in which U is lost to sediment via diffusion. In Fig. S2, we show results in which the model was initialized with the [U] and $\delta^{238}U$ characteristics of open-ocean seawater ([U] = 13.4nM and $\delta^{238}U$ = -0.39‰), and the degree of U drawdown at the base of the water column was varied by changing ν/k. The predicted co-variation trend between [U] and $\delta^{238}U$ becomes increasingly non-linear as U loss to the sediment increases. However, it is important to note that the $\delta^{238}U$ of dissolved U at the very base of the water column is a simple linear function of the degree to which U is drawn down by loss to sediment, relative to the initial open-ocean condition.

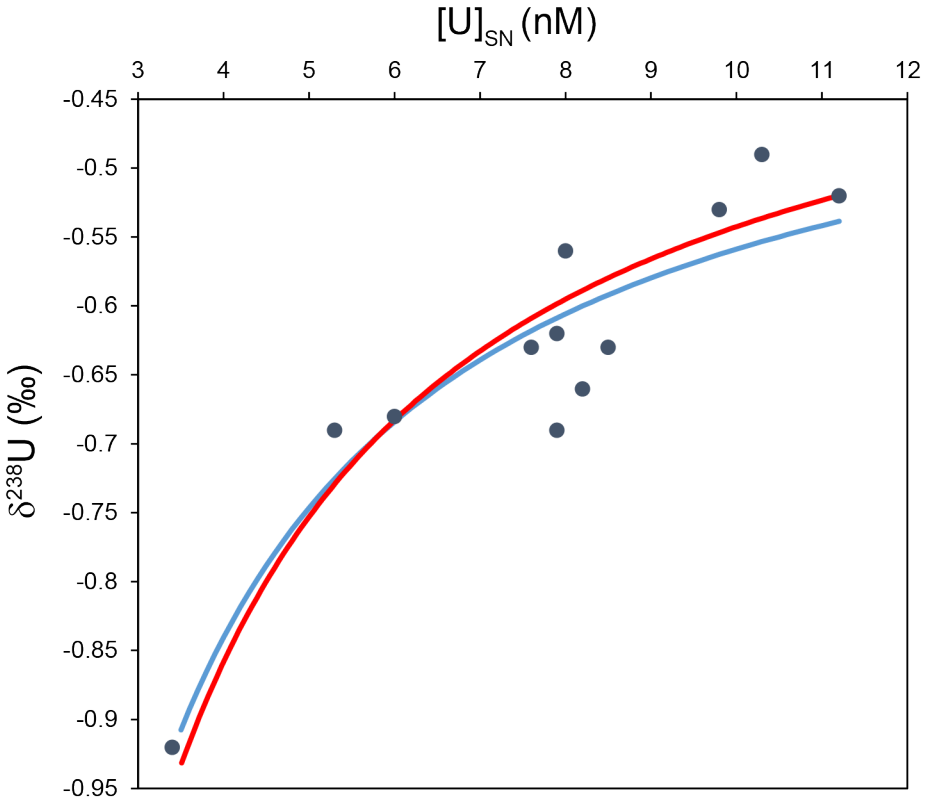

Fig. S1: U isotope systematics of Lake Rogoznica in February 2013. When initialised with the observed [U] and $\delta^{238}U$ properties of the top of the water column (top right), the one-dimensional water column model (red line) reproduces the degree of $\delta^{238}U$ variability expected when [U] is drawn down to ~3.5 nM at the base of the water column, due to diffusion-driven loss to the sediments. The model solution is virtually indistinguishable from a linear regression to the data ($\delta^{238}U$ versus 1/[U]) that describes the co-variation expected purely as the result of conservative mixing of U within the water column (blue line).

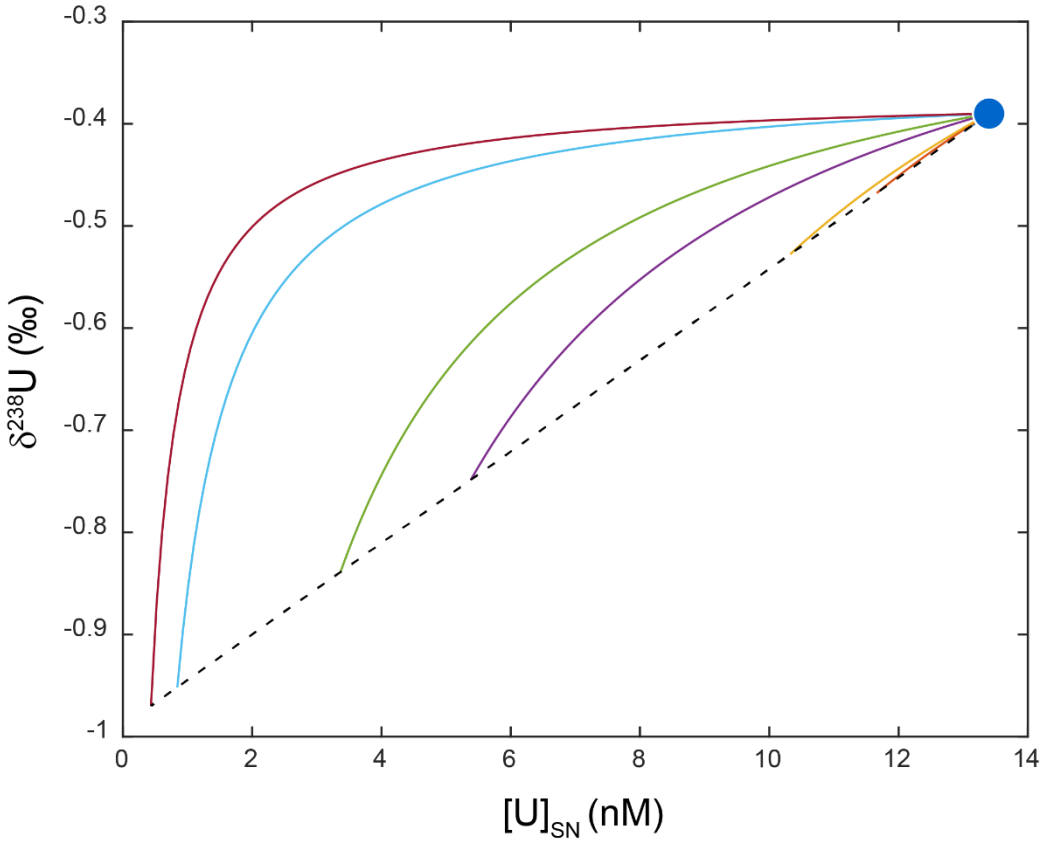

Fig. S2: U isotope systematics for varying degrees of U drawdown. Each curve represents the water-column co-variation between [U] and $\delta^{238}U$ predicted by the model for varying degrees of U drawdown at the base of the water column with an isotope effect of +0.6‰. The starting point (blue circle) represents open-ocean seawater. As can be seen, this relationship becomes increasingly non-linear as the [U] difference between the top and bottom of the water column increases. However, the isotope composition of dissolved U at the very base of the water column is a simple linear function of [U], i.e. of the extent to which U has been drawn down relative to the open-ocean initial of 13.4 nM.